Acta Pharmaceutica Sinica B 2021;11(3):632–650

Chinese Pharmaceutical Association
Institute of Materia Medica, Chinese Academy of Medical Sciences

Acta Pharmaceutica Sinica B

www.elsevier.com/locate/apsb
www.sciencedirect.com

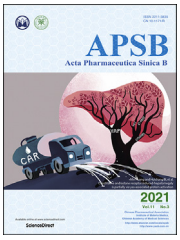

REVIEW

Diversity of the reaction mechanisms of SAM-dependent enzymes

Qiu Sun[*,†], **Mengyuan Huang**[†], **Yuquan Wei**

State Key Laboratory of Biotherapy, Cancer Center, West China Hospital, Sichuan University and Collaborative Innovation Center for Biotherapy, Chengdu 610041, China

Received 11 May 2020; received in revised form 30 July 2020; accepted 8 August 2020

KEY WORDS

SAM-dependent enzyme;
Catalytic mechanism;
Biocatalysis;
Nonmethylation reaction;
Methyltransferase

Abstract *S*-adenosylmethionine (SAM) is ubiquitous in living organisms and is of great significance in metabolism as a cofactor of various enzymes. Methyltransferases (MTases), a major group of SAM-dependent enzymes, catalyze methyl transfer from SAM to C, O, N, and S atoms in small-molecule secondary metabolites and macromolecules, including proteins and nucleic acids. MTases have long been a hot topic in biomedical research because of their crucial role in epigenetic regulation of macromolecules and biosynthesis of natural products with prolific pharmacological moieties. However, another group of SAM-dependent enzymes, sharing similar core domains with MTases, can catalyze nonmethylation reactions and have multiple functions. Herein, we mainly describe the nonmethylation reactions of SAM-dependent enzymes in biosynthesis. First, we compare the structural and mechanistic similarities and distinctions between SAM-dependent MTases and the non-methylating SAM-dependent enzymes. Second, we summarize the reactions catalyzed by these enzymes and explore the mechanisms. Finally, we discuss the structural conservation and catalytical diversity of class I-like non-methylating SAM-dependent enzymes and propose a possibility in enzymes evolution, suggesting future perspectives for enzyme-mediated chemistry and biotechnology, which will help the development of new methods for drug synthesis.

*Corresponding author. Tel.: +86 28 85421753; fax: +86 28 85164060.
E-mail address: sunqiu@scu.edu.cn (Qiu Sun).
†These authors made equal contributions to this work.

Peer review under responsibility of Chinese Pharmaceutical Association and Institute of Materia Medica, Chinese Academy of Medical Sciences.

https://doi.org/10.1016/j.apsb.2020.08.011

1. Introduction

S-adenosylmethionine (SAM) is a dominant metabolic intermediate and ubiquitous cofactor in all living organisms[1,2]. The majority of SAM-dependent enzymes are responsible for methylation and are generally called methyltransferases (MTases). SAM-dependent MTases are involved in many biopathways, including pathways involved in the modification of biopolymers (such as lipids, proteins and nucleic acids) and biosynthesis of small-molecule metabolites.

SAM-dependent MTases have long been a hot topic in biomedical research. Methylation of proteins and nucleic acids is of great significance in epigenetic regulation[3−5]. To date, considerable efforts have been made to develop therapeutic agents targeting DNA and protein MTases whose abnormal activity is thought to underlie the pathology of various diseases, such as cancer, diabetes, and Alzheimer's disease[6,7]. The significance of MTases is also underscored by their crucial roles in the biosynthesis and biocatalytic modification of natural products (NPs). NPs and their derivatives provide a large scope for fragment-based drug design and for skeleton modification of prolific pharmacological scaffolds, such as phenazine, benzoquinone, pyrimidine, porphyrin, flavonoid, and benzenediol lactone scaffolds[8−13]. These compounds exhibit great potential in the treatment of cancer, inflammation, Alzheimer's disease and many other human diseases[9−12]. Methylation is an indispensable intermediate step for diversification of the NP skeleton in biosynthetic pathways, exhibiting a preponderance in chemo-, regio- and stereo-specific synthesis and ecofriendly characteristics. Thus, a very large number of MTases have potential applications in the industrial synthesis of bioactive compounds[14−16]. For example, vanillin and isovanillin regioisomers can be generated by engineered catechol *O*-methyltransferases (COMTs) and the catechol 4-*O*-methyltransferases SafC[17]. One of the flavonoid derivatives, 7-*O*-methyl aromadendrin, can be obtained from *p*-coumaric acid by engineering SaOMT-2 in *Escherichia coli*[18]. A significant family of alkaloid benzylisoquinolines can be obtained by using 6-OMT, coclaurine NMT and 4′-OMT in cascade synthesis[19].

Intriguingly, there is a group of SAM-dependent enzymes that share highly similar core domains with MTases but catalyze diverse types of reactions such as decarboxylation, oxidation, cyclization and hydroxylation (Table 1[20−34]). In addition, radical SAM-dependent (RS) enzymes, which have been widely studied in radical chemistry, also exhibit the ability to catalyze multiple reactions[35−40]. In this review, we will discuss the structure, reaction and catalytic mechanism of multifunctional SAM-dependent enzymes and compare them with typical MTases in terms of structure and mechanism to provide detailed insight into the applications of these enzymes. This review covers the novel SAM enzymes with class I core domains and several typical radical SAM enzymes, which catalyze non-methylation reactions.

2. SAM-dependent enzymes

2.1. Classification and structure

The methyltransferase family is one of the superfamilies of SAM-dependent enzymes. Since the first structure of C5-cytosine-DNA-methyltransferases was obtained[41], MTases have been continuously studied. In general, MTases can be divided into five classes based on their structural topologies[42]. Class I MTases are characterized as having a full Rossmann fold with a seven-stranded β-sheet and flanking α-helices that form a doubly wound open $\alpha\beta\alpha$-sandwich, showing a central topological switch-point and a β-hairpin at the carboxyl end of the sheet (Fig. 1A). The glycine-rich (GxGxG or GxG) motif in the first β-sheet and a strongly conserved acidic residue at the end of β2-sheet are hallmarks of SAM binding. The auxiliary N-terminus is flexible for substrate recognition and polymerization in some cases. Class I MTases constitute one of the main groups of MTases involved in NP biosynthesis[13], and some SAM-dependent enzymes catalyzing the nonmethylation reactions of NPs (enzymes independent on the [4Fe-4S] cluster) also share similar core topologies with class I MTases, which will be discussed below. Very similarly, class IV MTases show half of the Rossmann fold but differ in the unique C-terminus that tucks back and forms a "knot" (Fig. 1D). Class II, III and V MTases exhibit considerably different topologies compared to class I MTases[42]. The class II MTases core domain is dominated by a long antiparallel β-sheet at the center of the enzyme flanked by groups of helices. SAM is bound to the RxxxGY motif, positioned in a shallow groove at the edge of β-sheet (Fig. 1B). The active site of class III MTases is anchored into a large cleft by two $\alpha\beta\alpha$-domains containing five β-strands and four helices in each domain, indicating a large pocket between the N- and C-terminal domains for substrate binding. SAM is tightly folded in the active site but does not bind to the GxGxG motif, which is also conserved in class III MTases (Fig. 1C). Class V MTases are composed of a series of β-strands and a knot-like C-terminus tucked under the surface loop. SAM is bound in the shallow cleft proximal to the C-terminus (Fig. 1E). Although these five classes of MTases comprise complete, partial or small Rossmann folds, they vary markedly in overall topologies, SAM conformation and binding manner.

Radical SAM (RS) enzymes belong to another superfamily responsible for methylation. They generate high-energy radical molecules that can methylate unreactive non-nucleophilic centers of substrates and catalyze a wide range of reactions in addition to methylation. This superfamily shares a common partial $(\alpha/\beta)_6$ TIM barrel fold or full TIM barrel in some cases, in which a β-sheet is anchored inside by peripheral α-helices, sharing a lateral opening manner at the active site[43]. This open β-sheet is covered by a C-terminal domain and part of the N-terminal domain (Fig. 2A and C). The [4Fe-4S] cluster is bound at the top of the partial TIM barrel core domain, stabilized by SAM and a highly conserved cysteine-rich motif in the loop following the β1-strand. A neighboring SAM molecule coordinates one Fe ion of the cluster through its amide nitrogen and carboxylate oxygen in a bidentate fashion, and the other three Fe ions coordinate with the cysteine residues in the cysteine-rich motif (Fig. 2B). SAM is also bound across the top of the barrel, stabilized by residues from several core β-strands. However, the wide dispersion of SAM binding hinders the identification of specific SAM-binding motifs beyond the previously identified glycine-rich region. Further details have been comprehensively discussed by Vey et al.[43] in a previous review.

Some SAM-dependent enzymes catalyze non-methylation reactions or multiple reactions without [4Fe-4S] clusters. They possess SAM as a cofactor and share similar core domains with MTases, especially the characterized Rossmann fold in class I MTases. The hydroxylase RdmB[21] has a Rossmann-like fold composed of a parallel five-stranded β-sheet surrounded by seven α-helices at the two opposite sides. The N-terminus with several α-helices is involved in dimerization. Cyclopropane fatty acyl

Table 1 The non-methylation reactions, sources and structure information of non-methylating SAM-dependent enzymes[20–34].

Reaction type		Enzyme	Source	Catalytic domain	Key ligand	PDB code	Ref.
Decarboxylation	Decarboxylation	HemN	*Escherichia coli*	Partial TIM barrel in N-terminus	[4Fe-4S] cluster, two SAMs	1OLT	20
	Decarboxylation and hydroxylation	RdmB	*Streptomyces purpurascens*	Class I MTases core domain (a Rossmann-like fold) in C-terminus	SAM	1XDS	21
Ring-opening reaction		ChuW	*Escherichia coli*	Partial TIM barrel in N-terminus	[4Fe-4S] cluster, two SAMs	–	22
Cyclization	Cyclopropanation	YtkT	*Streptomyces zelensis*	Partial TIM barrel in N-terminus	[4Fe-4S] cluster, two SAMs	–	23
		C10P	*Streptomyces zelensis*	Partial TIM barrel in N-terminus	[4Fe-4S] cluster, two SAMs	–	24
		CMASs (PcaA, CmaA1, CmaA2)	*Mycobacterium tuberculosis*	Class I MTases core domain (a Rossmann-like fold) in C-terminus	SAM, a bicarbonate ion	1L1E, 1KPG, 1KPI	25
		CFASs	*Lactobacillus acidophilus* and *Escherichia coli*	Class I MTases core domain (a Rossmann-like fold) in C-terminus	SAM, a bicarbonate ion	5Z9O, 6BQC	26, 27
	SAM cyclization	VioH	*Cysotobacter violaceus*	Class I MTases core domain (a Rossmann-like fold) in C-terminus	SAM	–	28
	Formation of double bond and bis(spiroacetal)	SlnM	*Streptomyces albus*	–	SAM	–	29
	Carbocation-mediated cyclization	TleD	*Streptomyces blastmyceticus*	Class I MTases core domain (a Rossmann-like fold) in C-terminus	SAM	5GM2	30
	[4+2] cycloaddition	SpnF	*Saccharopolyspora spinosa*	Class I MTases core domain (a Rossmann-like fold) in C-terminus	SAM	4PNE	31
	Pericyclization	Lepl	*Aspergillus flavus*	Class I MTases core domain (a Rossmann-like fold) in C-terminus	SAM	6IX5	32
Methylation, dehydrogenation and chelation		CysG	*Salmonella enterica*	Class III MTases core domain in C-terminus and dehydrogenase-ferrochelatase module in N-terminus	SAM, NAD+	1PJS	33
Methylation, epoxidation and isomerization		PsoF	*Aspergillus fumigatus*	SAM-containing MTase domain and FAD-containing monooxygenase domain	SAM, FAD	–	34

–Not applicable.

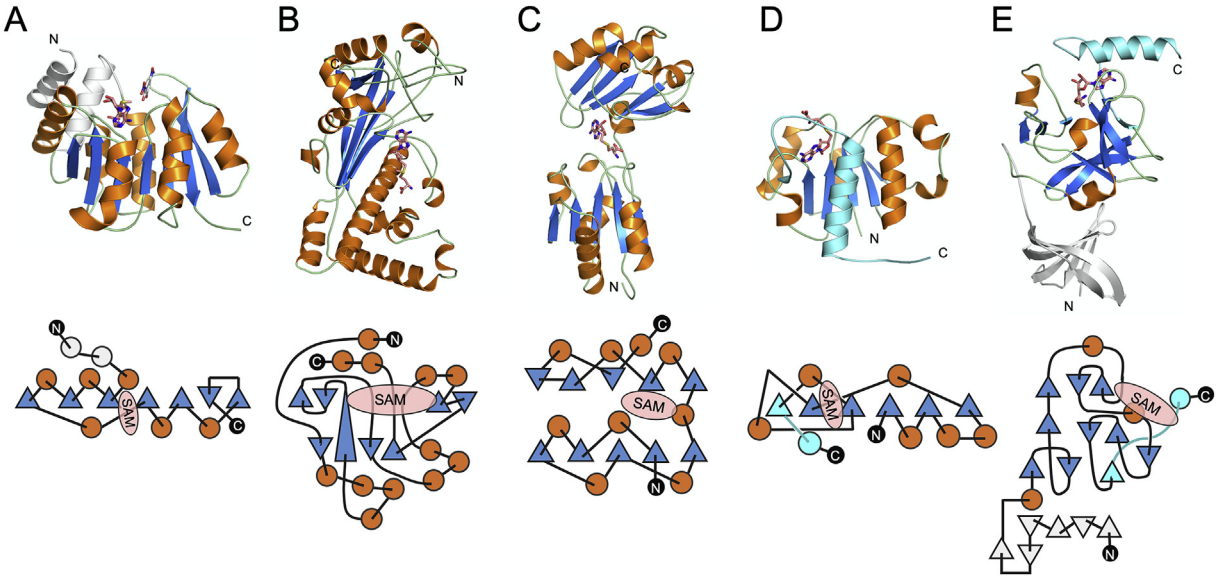

Figure 1 The five classes of SAM-dependent MTases. The core domain and primary architecture of the representative enzyme in each case are shown in cartoons (top) and topology diagrams (bottom). (A) Class I MTases, exemplified by COMT (PDB: 1VID): the Rossmann fold with a seven-stranded β-sheet and flanking α-helices in the C-terminus is defined as the core domain in this class. The auxiliary N-terminus (colored in grayish-white) is specific for substrate recognition and polymerization. (B) Class II MTases, exemplified by MetH (PDB: 1MSK): the key characteristic of this class is a long antiparallel β-sheet flanked by groups of helices. (C) Class III MTases, exemplified by CbiF (PDB: 1CBF): two $\alpha\beta\alpha$-domains formed in the N- and C-termini anchor the active site, providing a sufficiently large pocket for large substrates and SAM. (D) Class IV MTases, exemplified by YibK (PDB: 1MXI): the partial Rossmann fold is similar to that of class I MTases but differs in the knot-like C-terminus (colored in cyan), which tucks back and inserts itself into the space between a α-helix and a β-strand. (E) Class V MTases, exemplified by Set7/9 (PDB: 1O9S): the structure is mainly composed of a series of β-strands with several flanking α-helices. The C-terminus tucks back to form a "knot" (colored in cyan). In both the cartoon and topology diagrams, α-helices and β-strands in the characteristic domain are colored orange and blue, knot-like domains are colored cyan, variant domains are colored grayish-white, and SAM molecules are colored pink.

phospholipid synthase (CFAS)[26] shares a C-terminal $(\alpha/\beta)_7$-fold, and the phospholipids are located in a tunnel, extending from the surface between the N- and C-termini to the central cleft. Moreover, TleD[30], SpnF[31] and LepI[32], which catalyze cyclization, all share a typical Rossmann fold in the C-terminus with an extensive N-terminus for dimerization and a tightly covered active site. Nevertheless, these enzymes show some differences in the conformation and length of the N-terminal domain (Fig. 5). The N-terminal domain in SpnF does not insert itself into another subunit but simply anchors its own active site[31], while LepI has a relatively large N-terminus for dimerization in a swapped manner and a completely compacts the substrate cavity *via* a leucine-rich coiled coil[32].

2.2. *General catalytic mechanisms*

2.2.1. *S_N2 or S_N2-like methylation*

In the methylation of natural products, S_N2 nucleophilic replacement is one of the most universal synthetic mechanisms (Fig. 3A). The proper distance and orientation of the nucleophilic center in the vicinity of the electron-deficient methyl moiety are prerequisites for S_N2-like methylation[13]. The methyl donor atom in SAM and acceptor atom in the substrate are located in a linear arrangement as required by the methyl transfer reaction, which is achieved by reorientation of adjacent residues or flexible loops of the enzyme upon binding. The reaction is followed by a nucleophilic attack on the active methyl group in SAM, inducing the cleavage of C−S bonds. S_N2 or S_N2-like methylation in natural product biosynthesis relies on three different mechanisms[13]. The first mechanism, which is associated with proximity and desolvation, was originally discovered in salicylic acid carboxyl methyltransferase[44]. For this mechanism, the catalytic reaction does not require residues or components in the solvent, depending instead on the proper environment being formed by the architecture of the active site. In the active site of DnrK, the possible general base Tyr142 is observed to be in proximity to the substrate, but mutagenesis of Tyr142 does not have a substantial effect on the catalytic reaction[45], indicating that DnrK uses the proximity- and desolvation-based mechanism to perform methylation (Fig. 3B). The second mechanism, called general acid/base-mediated catalysis, uses residues in optimal orientation (histidine, arginine or other basic residues, as usually observed) to subtract hydrogen atoms from substrates, for instance, Arg201 and Tyr78 in Coq5[46], His120 in CouO[47], Tyr226 in CbiL[48] and Arg111 in NirE[49]. In NirE, Arg111 acts as an essential base to deprotonate C-20 of substrate and promotes electron transfer, facilitating the subsequent methylation of C-2 of substrate. Glu114 is also essential for correction of the orientation of Arg111 (Fig. 3C). While, instead of using residues in enzymes as general bases, cyclopropane fatty acyl phospholipid synthases mostly adopt a novel mechanism that depends on bicarbonate as a base[26]. The third mechanism is referred to as the metal-dependent mechanism (Fig. 3D). Metal ions in the active site serve as general bases for deprotonation of the substrate through coordination with the substrate or alter the pK_a of the phenolic hydroxyl group and promote deprotonation. Caffeoyl coenzyme A 3-*O*-

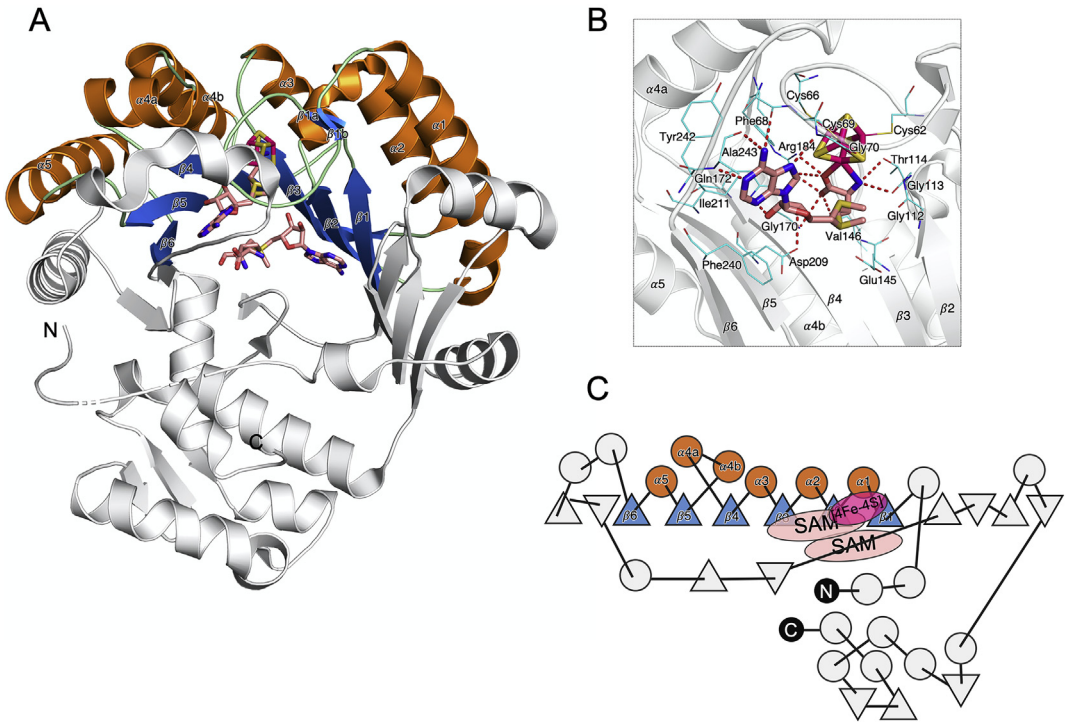

Figure 2 Overall structure, close-up view and topology diagram of a representative radical SAM enzyme (HemN, PDB: 1OLT) are shown in a cartoon and a topology diagram. The core TIM barrel is defined as the region from the N-terminus of the strand (β1) leading to the cluster-binding loop to the C-terminus of the sixth strand (β6). In the representative enzyme HemN[20], the core TIM barrel containing residues from Leu53 to Asn241 is highlighted[43]. (A) Overview of HemN. The partial $(\alpha/\beta)_6$TIM barrel is conserved in the majority of radical SAM enzymes. The special α4a protrudes from the partial TIM barrel, and its C-terminus is oriented toward a cluster-binding loop (between β1 and α1). (B) Close-up view of the [4Fe-4S] cluster and SAM binding mode. Three cysteines (Cys62, Cys66 and Cys69 in HemN) on the loop following the first main strand in the TIM barrel are conserved for cluster binding and coordinating with three Fe ions (colored in magenta), which is referred to as the cysteine-rich motif. The amide nitrogen and carboxylate oxygen of SAM coordinate to the fourth Fe ion. The SAM adjacent to the cluster binds at the top of the TIM barrel, and the glycine-rich motif (Gly112, Gly113 and Thr114 in HemN) is defined in many radical SAM enzymes, but other SAM-binding motifs are difficult to identify on account of the large overlap of the SAM-binding regions in different enzymes. Here, we labeled both hydrophilic and hydrophobic residues of one SAM-binding region in HemN. The second SAM molecule is present in some cases, such as HemN, BioB and LipA[43], but the binding mode is not discussed here. (C) Topology diagram of HemN. In both the cartoon and topology diagram, α-helices and β-strands in the TIM barrel are colored orange and blue, variant domains are colored grayish-white, SAM is colored pink, Fe ions in the cluster are colored magenta, S atoms are colored yellow, residues are colored cyan, and hydrogen bonds are labeled with red dashed lines.

methyltransferases (CCoAOMT) follows this mechanism, in which a Ca^{2+} ion alters the pK_a of the hydroxyl group and assists in the formation of an oxyanion adjacent to the electron-deficient methyl group on SAM, thereby promoting subsequent methylation[50].

2.2.2. *Radical-based reactions*

Although many biological methylations can be achieved *via* S_N2 or S_N2-like replacement, an increasing number of enzymatic methylations have been reported to proceed *via* radical-based mechanisms[43,51]. At the start of the enzymatic reactions, one coordinated SAM molecule is cleaved to yield 5′-deoxyadenosyl radical (5′-dAdo•) as a potent oxidant. 5′-dAdo• initiates various reactions through two pathways: 5′-dAdo• directly activates the substrate and drives the subsequent reactions or abstracts the hydrogen from the methyl group of the second SAM molecule in the enzyme to form radical SAM, yielding 5′-deoxyadenosine (5′-dAdoH) at the same time. The radical SAM then acts on the substrate and drives various reactions (Scheme 1). Highly active radical intermediates dramatically enrich the reactions catalyzed by radical SAM enzymes, but great effort is needed to reveal the underlying mechanism to increase efficiency and decrease the formation of byproducts by radical intermediates.

3. Nonmethylation reactions catalyzed by SAM-dependent enzymes

3.1. *Decarboxylation*

In 2003, Layer et al.[20] determined the crystal structure of HemN, which functions as an oxygen-independent coproporphyrinogen III oxidase during heme biosynthesis. HemN combines two SAM cofactors and an iron-sulfur cluster. The structure of the HemN complex shares the three-quarter-barrel catalytic domain, harboring two SAM cofactors and a [4Fe-4S] cluster in a flattened loop. The active site inside the TIM barrel with a conserved cysteine motif shields the aggressive radical intermediates from the surrounding medium. Variation in the basic architecture may disrupt the selective binding of the substrate and cofactor, leading to correct binding of both large and small substrates[20]. Initially, it

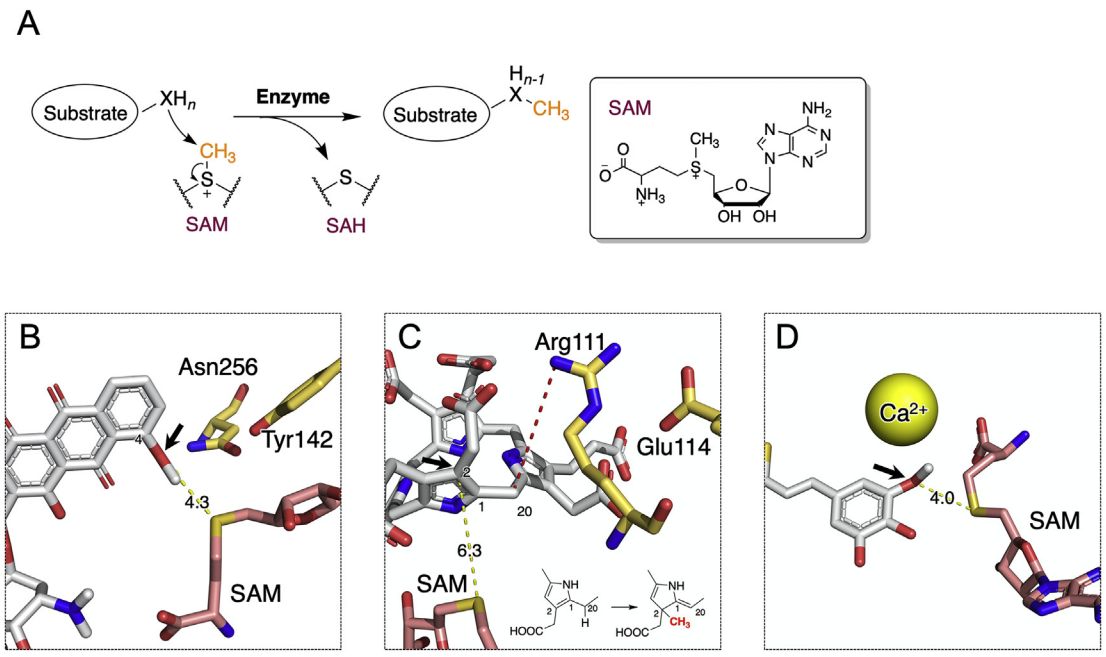

Figure 3 Mechanism of S_N2 or S_N2-like methylation. (A) General reaction performed by SAM-dependent MTases. Positively charged SAM acts as a methyl donor and provides a methyl group. The electron-sufficient atom attacks the methyl group, initiating S_N2-like replacement and inducing cleavage of the C−S bond. Finally, SAH is released during the production of a methylated substrate. (B) The "proximity and desolvation" mechanism, exemplified by DnrK[45]. Methylated oxygen is in proximity to the sulfonium group of SAM at a distance of approximately 4.3 Å (distance shown in yellow). Asn256 is supposed to assist substrate stabilization. Tyr142 is adjacent to a reactive oxygen species (O-4, indicated by the black arrow) but does not have a substantial effect on the catalytic rate, indicating that DnrK catalyzes methylation through a "proximity and desolvation" mechanism. (C) The general acid/base-mediated catalytic mechanism, exemplified by NirE[49]. Arg111 acts as a general base to deprotonate the hydrogen on C-20 of substrate, driving the S_N2-methyl transfer from SAM to C-2. Glu114 is important for correction of the orientation of Arg111. The present structure may not reflect the real position in the native enzyme because of the absence of SAM, resulting in a relatively large distance between the C-2 and S atoms in SAH (*S*-adenosylhomocysteine). Further details about the substrate conformation and residue orientation have been discussed in original research[49]. (D) The metal-dependent mechanism, exemplified by CCoAOMT[50]. Ca^{2+} ions in the active site alter the pK_a of the hydroxyl group and drive nucleophilic attack on the methyl group of SAM. In the stick view, substrates are colored grayish-white; SAM or SAH is colored pink; key residues and metal ions are colored yellow; the distance between S atoms and reactive atoms is labeled as a yellow dashed line; the hydrogen bond is labeled as a red dashed line; and reactive atoms in substrates are indicated by black arrows.

was believed that two bound SAMs produce two radical intermediates and are involved in two decarboxylation reactions[52,53], but this proposed mechanism does not perfectly explain the indispensable role of the second SAM molecule. A newly reported mechanism[54] clearly explains the role of the two SAM molecules in oxidative decarboxylation (Scheme 2A). One SAM molecule forms a 5′-dAdo• radical and abstracts a hydrogen atom from the methyl group of another SAM. The resulting radical SAM then abstracts the β-hydrogen atom of the carboxylate and enhances the release of carbon dioxide to form a terminal olefin. Another enzyme, HemW of *Lactococcus lactis*, shares 28% identity with HemN of *E. coli*[55,56], but unlike HemN, this enzyme cannot perform heme biosynthesis and shows no activity for oxidative decarboxylation. In 2018, Haskamp et al.[57] reported that HemW harbors two SAM molecules and a [4Fe-4S] cluster, and is present as a dimer upon cluster binding. They also found that HemW functions in heme trafficking, triggering the release of heme from HemW in the presence of membranes and acting as a heme chaperone[57,58]. Additionally, NirJ, AhbC/D, and CgdH also catalyze oxidative decarboxylation or assist the reaction with the aid of two SAM molecules and a [4Fe-4S] cluster[59,60]. They show sequence similarity and are responsible for the biosynthesis of heme d_1, heme and protoheme.

Anthracyclines are a series of natural compounds with aromatic polyketides produced by *Streptomyces* bacteria[62,63] and are usually used as anticancer drugs[64]. The biosynthesis of anthracyclines involves various reactions, including glycosylation, hydroxylation, decarboxylation and methylation, catalyzed by numerous enzymes[62,63]. DnrK and RdmB are two of these enzymes and are responsible for methylation and hydroxylation, respectively[45,65]. RdmB, an aclacinomycin-10-hydroxylase, is a methyltransferase homolog that simultaneously catalyzes decarboxylation and hydroxylation with dependence on SAM, and this reaction is a key step in the biosynthesis of the polyketide antibiotic β-rhodomycin[21]. The overall structure of RdmB shows a C-terminus containing a Rossmann-like fold formed by a five-stranded β-sheet and seven α-helices and an auxiliary N-terminus for dimerization. SAM is bound by a glycine-rich motif next to the substrate but is oriented in an unsuitable position for methyl transfer, demonstrating the impossibility of transmethylation. Arginine-assisted decarboxylation is the initial reaction in RdmB. Then, the substrate with large aromatic rings is further stabilized

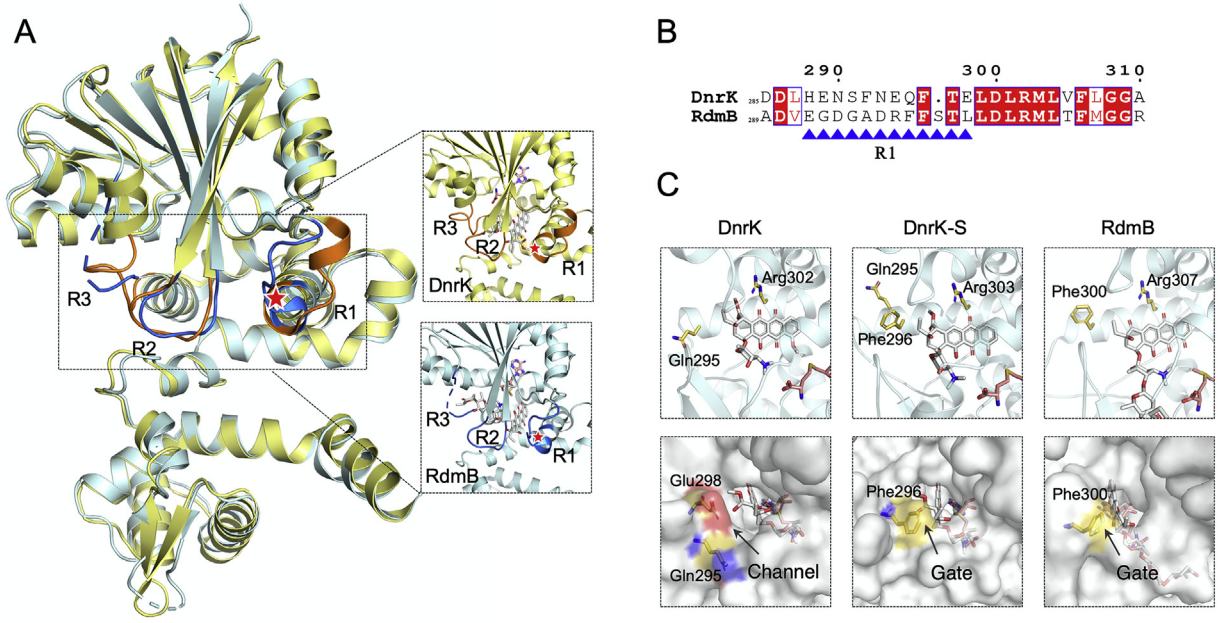

Figure 4 (A) Structural alignment and close-up views of DnrK (PDB: 1TW3) and RdmB (PDB: 1XDS). Variable regions around active sites are colored orange and blue for DnrK and RdmB respectively. Asterisks indicate the "gate" residues (Phe300 in RdmB). (B) Sequence alignment of residues around variable region (R1). The pairwise alignment is performed by EMBOSS needle and edited by ESPript[61]. (C) Close-up views of enzymes in cartoon (top) and surface (bottom) depictions show key residues in the active sites of DnrK, DnrK-S (PDB: 4WXH) and RdmB. Substrates are colored grayish-white; the cofactor SAM or SAH is colored pink; and residues are colored yellow.

by several hydrophobic residues targeting the vicinity of C-10 of the substrate, forming a cage for accommodating lone-pair electrons of oxygen and then generating a hydroperoxide. After the release of the substrate, a reductant from the enzyme reduces the hydroperoxide to a hydroxy group (Scheme 2B). RdmB shares 52% sequence identity and a similar three-dimensional structure with DnrK (an *O*-MTase involved in the biosynthesis of the anthracycline daunorubicin), with differences in three variable regions around the active sites (R1, R2 and R3 shown in Fig. 4A). Grocholski et al.[66] used chimeragenesis to explore why Dnrk and RdmB present almost the same structure but totally different functions[45,65]. They inserted an additional serine (Ser297) in the active site R1 of DnrK (Fig. 4A and B), and the variant DnrK-Ser (DnrK-S) exhibited complete reversal of the DnrK activity from methylase to monooxygenase. The structure of the variant DnrK-S shows a conserved phenylalanine with a similar orientation in both DnrK-S (Phe296) and RdmB (Phe300), but there is a distinct glutamine (Gln295) in DnrK at the same position (Fig. 4C). It is proposed that the phenylalanine serves as a gate that closes the channel and prevents solvent entry into the active cavity, and under this condition, water-assisted neutralization of the carbanion formed after decarboxylation would not occur in DnrK-S and RdmB (Scheme 2B). The negative charge of the carbanion is then stabilized by the polyphenolic moiety and the adjacent positive charge of SAM or its analog sinefungin. This delocalization of electrons helps in substrate-assisted activation of oxygen to overcome the similar spin barrier, similar to the manner in which other cofactor-independent monooxygenases work[67–70]. Upon completion of oxidation, the peroxy-substrate is released and reduced by the reagent outside the active site cavity. Notably, C-10 decarboxylation may occur, leading to the formation of the carbanion in both native DnrK and RdmB. This process is initiated by Arg302 in DnrK and Arg307 in RdmB, but the phenylalanines (Phe298 in DnrK-S and Phe300 in RdmB) and glutamine (Gln295 in DnrK) are crucial modulators that determine whether water-assisted neutralization of the carbanion occurs and further determine whether the enzyme functions as a methyltransferase or monooxygenase (Scheme 2B). This reversal of activity caused by chimeragenesis greatly broadens the scope of application and will inspire further research for protein engineering and antibiotic reform.

3.2. *Ring-opening reaction*

In heme metabolism, the degradation of heme is also of great significance for iron homeostasis and cell signals in diverse physiological and pathological processes[71,72]. Modification of heme scaffolds may be a potential strategy for modification of drugs with similar skeletons. The radical-based enzymes ChuW in *E. coli* O157:H7 and HutW in *Vibrio cholerae* are involved in this pathway[73,74]. ChuW catalyzes the degradation of heme in an oxygen-independent manner *in vitro*, resulting in the ring-opening of tetrapyrrole and the liberation of iron aided by two SAM molecules[22]. The catalytic mechanism of degradation is proposed to be consistent with the HemN-like radical process, in which the first SAM molecule is activated through homolytic cleavage and the subsequent 5′-dAdo• abstracts a hydrogen atom from another SAM molecule (SAM_2) to yield 5′-dAdoH. Then, the radical SAM attacks the substrate and initiates methyl transfer and rearrangement of the porphyrin ring, leading to iron release and ring opening (Scheme 3). ChuW utilizes a radical SAM system to provide the oxidant in an anaerobic environment instead of oxygen in aerobic spaces. Initially, ChuW was annotated as HemN, but this annotation was refuted based on evidence that ChuW could not rescue the function of HemN in HemN knockout *Salmonella enterica*[74,75]. Interestingly, both of these proteins are

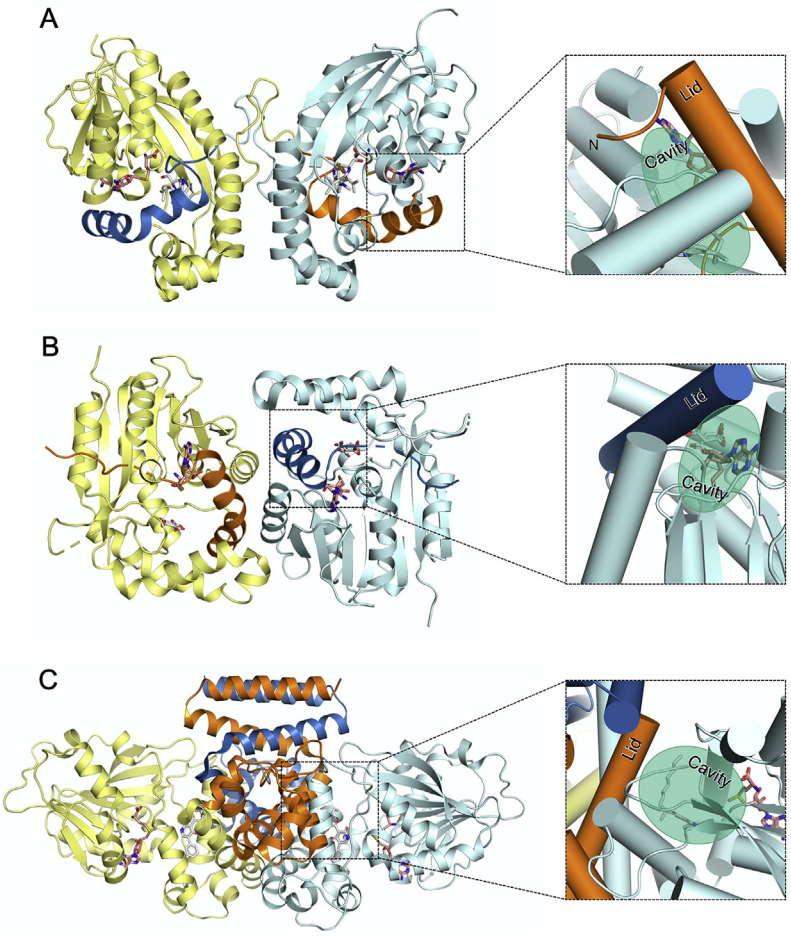

Figure 5 Overall dimeric structures (left) and close-up stereo views (right) of (A) TleD (PDB: 5GM2), (B) SpnF (PDB: 4PNE) and (C) LepI (PDB: 6IX5). One subunit in the dimer is colored light yellow and orange; the other is colored light cyan and blue. Additional N-termini acting as lids to compact the active site are underscored in orange and blue in each subunit; the substrate and cofactor are colored grayish-white and pink, respectively; the green circles show the substrate cavity of each enzyme.

crucial in the metabolism of heme and share similar functional domains, but HemN is responsible for the formation of heme, whereas ChuW catalyzes the degradation of heme; further structural exploration is needed to determine the key residues for catalysis.

3.3. Cyclization

Members of the spirocyclopropane family, including yatakemycin (YTM), CC-1065 gilvusmycin, duocarmycin A and duocarmycin SA[76–80], share a highly active cyclopropane moiety, which indicates their exceptionally potent cytotoxicity[81,82]. The coplanarity of the three carbon atoms, short and π-like C−C bonds and strong C−H bonds of the cyclopropane moiety make it a good choice for improvement of metabolic stability and brain permeability and prompt alteration of pK_a during drug discovery[9]. Many agents containing cyclopropane have entered the clinical phase in targeted tumor therapy and infectious disease research[9,83–85]. However, difficulties in regioselectivity are a constant concern in chemical synthesis, and multisubstituted cyclopropanes are no exception[86]. Based on the critical role and challenging synthesis of these compounds, biosynthesis of cyclopropane continues to attract attention. In the biosynthesis of YTM, YtkT catalyzes the formation of a spirocyclopropane ring through radical cyclopropanation at the sp^2-carbon of the aromatic ring[87] (Scheme 4A). YtkT is a radical SAM enzyme that catalyzes cyclopropanation of YTM-T to yield YTM and shares sequence identity with HemN[23]. It has a conserved cystine-rich motif, which is a classic motif for [4Fe-4S] cluster binding. In addition, the HemN-like radical enzyme C10P[24] and methyltransferase C10Q[88] constitute a cyclopropanase system for cyclopropanation of CC-1065. C10P is the first to participate in the reaction. One SAM molecule in proximity to the metal cluster forms 5′-dAdo• and abstracts a proton from the methyl group of another SAM molecule. Then, the radical SAM adds to C-11 in substrate **1** and generates radical intermediate **2**, which abstracts a proton from the solvent and generates **3** (Scheme 4B). Next, assisted by His138 in C10Q, the hydroxy group at the 6-position of **3** is deprotonated, which leads to electron rearrangement, followed by the formation of cyclopropane *via* an intramolecular S_N2 cyclization mechanism.

SAM-dependent enzymes are also used in the conversion of lipid double bonds to cyclopropanes, such as the cyclopropanase Jaw5[89,90], cyclopropane mycolic acid synthases (CMASs)[25,91] and cyclopropane fatty acid synthases (CFASs)[92–94]. Three CMASs (PcaA, CmaA1 and CmaA2)[25] and CFASs[26,27] show similar class I MTase core domains in the C-terminus for substrate binding and catalysis but differ in the N-terminal domain for lipid binding. The

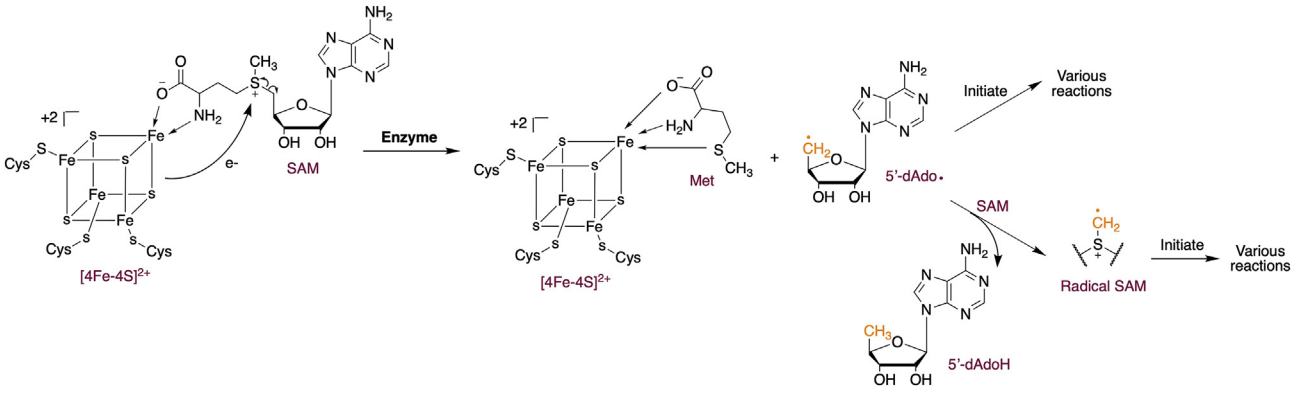

Scheme 1 Mechanism of radical-SAM-based reactions. The C−S bond of the SAM molecule is disrupted by homolytic cleavage, and 5′-dAdo• is obtained. 5′-dAdo• then directly initiates the subsequent reaction or abstracts hydrogen from the second SAM to yield radical SAM and drives the subsequent reactions indirectly.

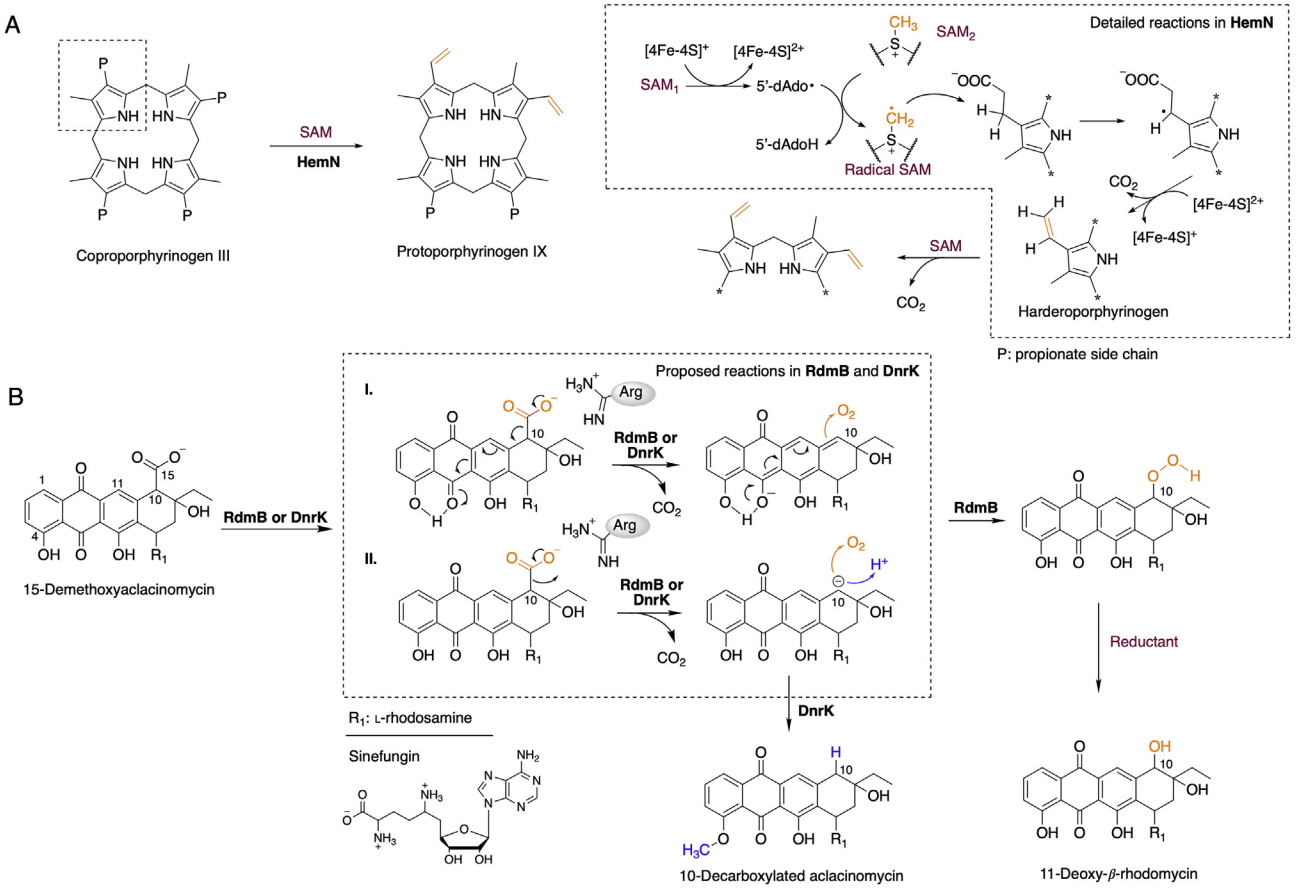

Scheme 2 Reactions catalyzed by HemN and RdmB. (A) Proposed radical-mediated decarboxylation catalyzed by HemN. (B) The proposed arginine-mediated decarboxylation is catalyzed by both RdmB and DnrK. Hydroxylation and methylation are catalyzed by RdmB and DnrK, respectively. Two possible pathways of oxygenation are shown in the dashed rectangle, and the corresponding atom in RdmB-mediated oxygenation is colored orange; the corresponding atom in DnrK-mediated neutralization and methylation is colored blue. Ovals in gray represent residues in enzymes. Proposed electron transfers are indicated by curved arrows.

linkage between the two domains is indicative of a hinge that hides the substrate in the active site and is responsible for the closing or opening of the active site for catalysis and substrate release[27]. A bicarbonate ion is present in the active site of some CMASs and CFASs, acting as a general base to deprotonate the hydrogen of the carbocation intermediate, and is a key component in CMAS- and CFAS-mediated cyclopropanation (Scheme 4C).

Vioprolides A−D make up a class of antifungals with potent immunomodulatory effects produced by the myxobacterium *Cysotobacter violaceus* Cb vi35[95]. Vioprolides A and C possess a

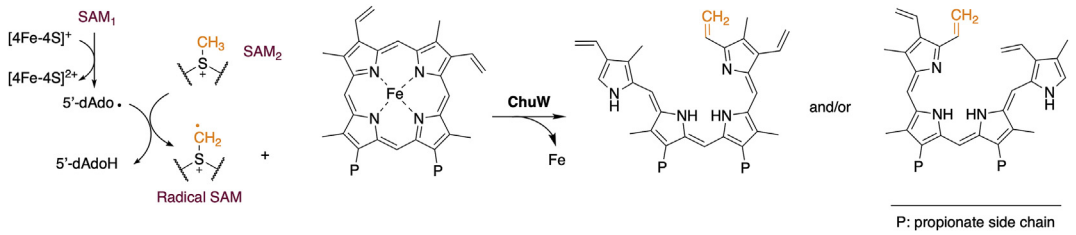

Scheme 3 Ring-opening reaction catalyzed by ChuW.

4-methylazetidinecarboxylic acid (MAZ) key moiety. However, the MAZ moiety is rarely found in natural products, except in bonnevillamide A, which is isolated from *Streptomyces* sp. GSL-6B[96]. The class I MTase-like enzyme VioH catalyzes the S_N2 reaction in SAM to form azetidinecarboxylic acid (AZE), followed by a methylation reaction catalyzed by the radical SAM enzyme VioG to yield the MAZ moiety[28,97] (Scheme 4D). It is proposed that VioH deprotonates the amino group of SAM and stimulates the intermolecular cyclization of SAM molecules, but the structural details need to be further clarified.

Salinomyzin is a polyether antibiotic containing a bis(spiroacetal) core structure. The unique structure endows it with the ability to chelate metal ions and outstanding potency in killing cancer stem cells[98–100], indicating the significance of understanding its biosynthetic mechanism. The formation of its Δ[18,19] double bond and bis(spiroacetal) is catalyzed in an unprecedented manner by the SAM-dependent enzyme SlnM[29]. SlnM is moderately homologous to TcmP, an *O*-MTase[101], and contains a glycine-rich motif for SAM binding[13,102,103]. Further biochemical studies have elucidated the indispensability of SAM and acidic residues for completion of the reaction. Initially, the movement of electrons from the oxygen atom on C-17 to C-19 enhances the acid-assisted dehydration process and facilitates the attack on C-17 by the hydroxy group on C-13, converting the corresponding cyclohexanone to the desired products (Scheme 5A). The electropositive sulfur atom of SAM increases the acidity of amino

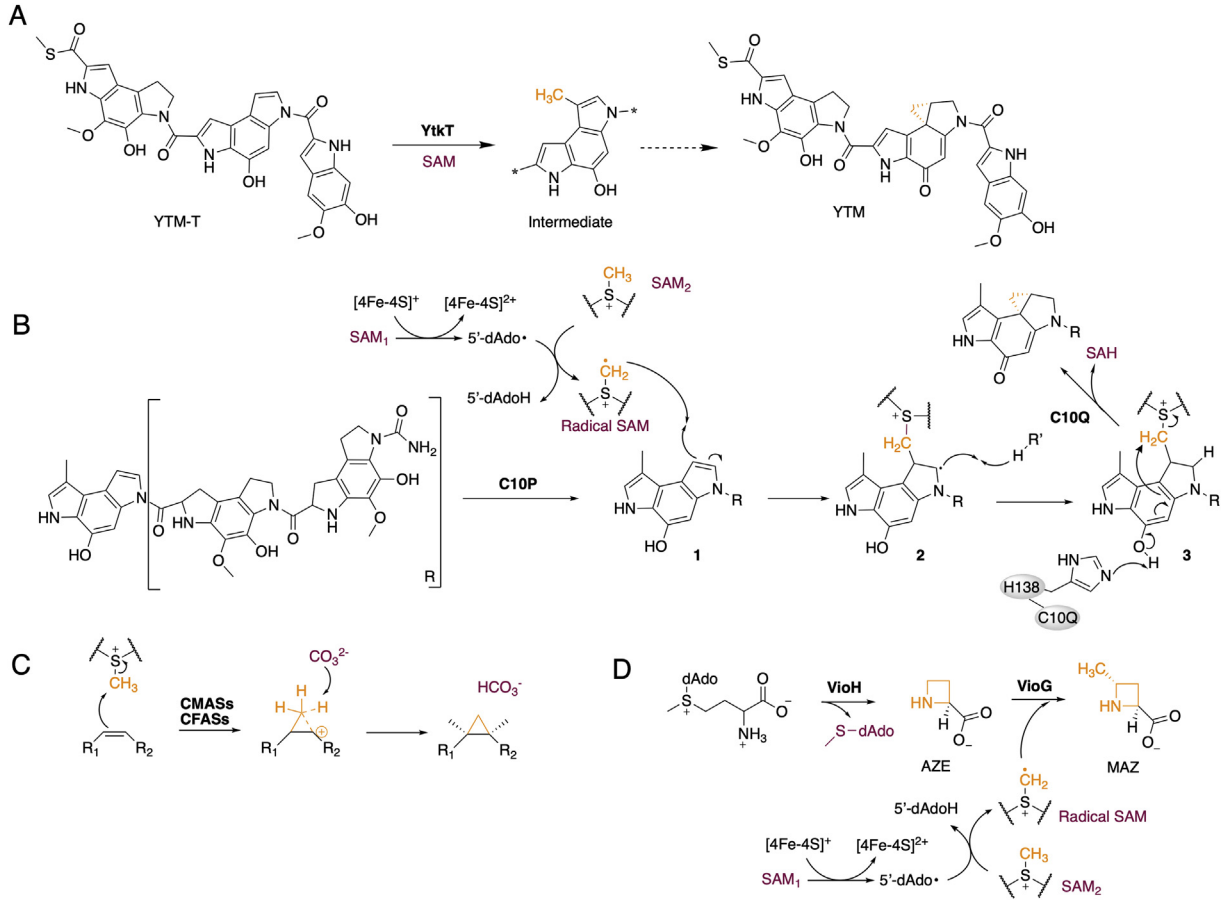

Scheme 4 Cyclization catalyzed by SAM-dependent enzymes. (A) Methylation and cyclopropanation catalyzed by YtkT. (B) Proposed mechanism of radical-mediated cyclopropanation catalyzed by C10P and C10Q. (C) Proposed mechanism of bicarbonate-mediated cyclopropanation catalyzed by CMASs and CFASs. (D) Cyclization and methylation catalyzed by VioH and VioG.

acids around the active site, presumably by loss of the activation of the neutrally charged SAH and the remaining function of the positively charged sinefungin (analog of SAM).

Teleocidin B possesses an indolactam-based alkaloid and is a potent protein kinase C activator[104]. Terpene cyclization usually follows a cationic mechanism as an initial step in organisms. The carbocation is usually produced by the release of a pyrophosphate, protonation of an epoxide ring or carbon−carbon formation[104–106]. In the biosynthesis of teleocidin B from teleocidin A1 (TelA1), TleD catalyzes the formation of carbonium ions by methyl transfer from SAM and then initiates terpene cyclization[107] (Scheme 5B). TleD forms a hexamer domain-swapped pattern and shares an additional N-terminal α-helix inserted into the typical class I MTase fold domain of its adjacent subunit[30]

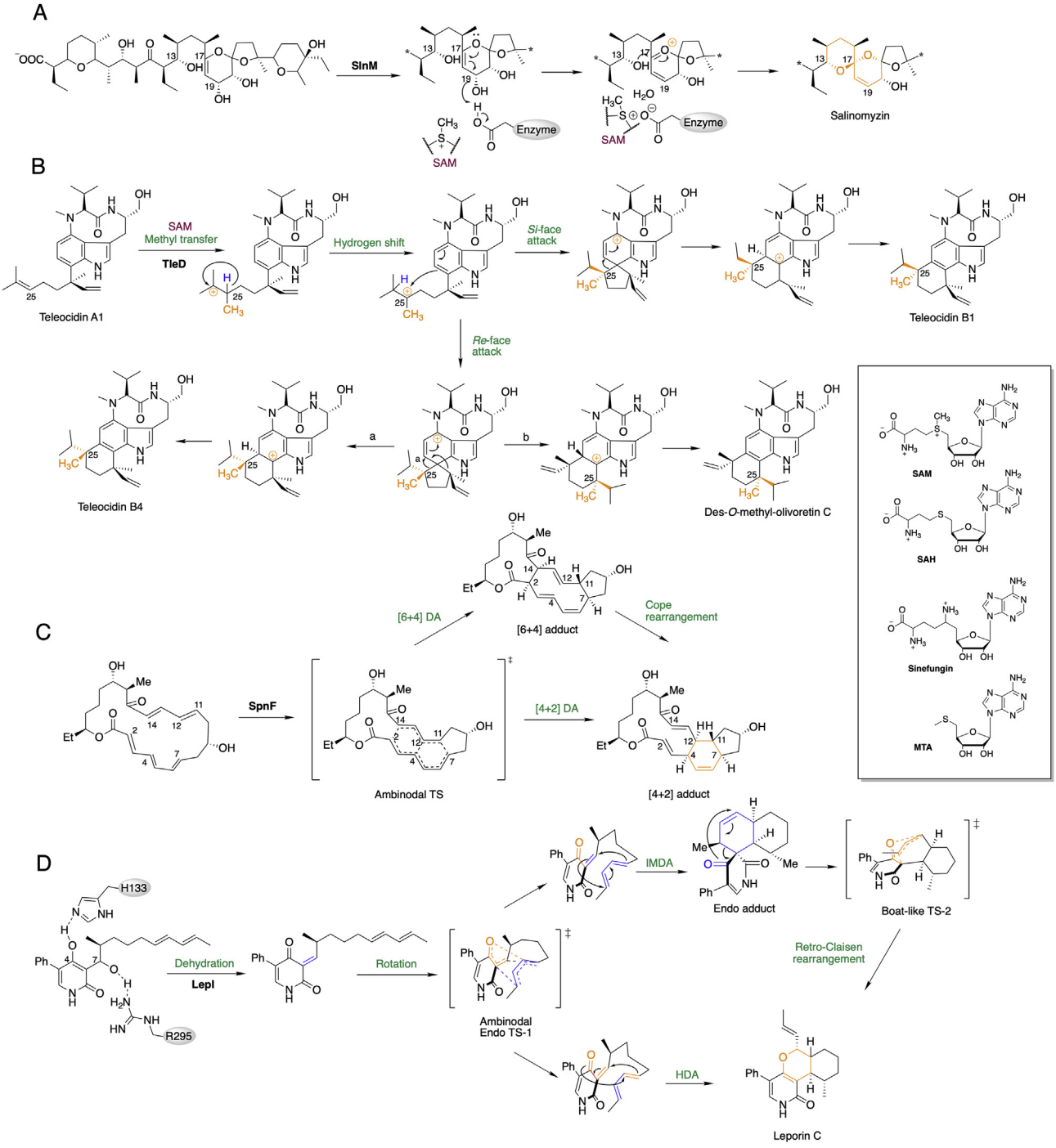

Scheme 5 Multiple reactions catalyzed by the indicated enzymes. (A) Proposed mechanism for the formation of the spiro-ring catalyzed by SlnM. (B) Proposed mechanism of carbocation-mediated cyclization catalyzed by TleD. (C) [4+2] and [6+4] cycloaddition and Cope rearrangement catalyzed by SpnF. (D) Dehydration, branch pericyclization and rearrangement catalyzed by LepI. SAM and its analogs are shown in the box. Ovals in gray represent residues or corresponding enzymes. Proposed electron transfers are indicated by curved arrows. MTA, 5′-deoxy-5′-(methylthio) adenosine; DA, Diels–Alder reaction; IMDA, intramolecular Diels–Alder reaction; HAD, hetero-Diels–Alder reaction.

(Fig. 5A, left). The additional N-terminal α-helix anchors the active site to form a compact pocket that can accommodate only TelA1, while water molecules cannot enter. Glu153 and Glu181 form hydrogen bonds with the substrate, promoting its adoption of the proper conformation. Tyr21 serves to maintain the correct position of the additional N-terminal α-helix, which may facilitate the generation of the enclosed active site. Notably, the geranyl group of TelA1 shows alternative rotation, which might lead to two conformations (Scheme 5B), namely, a *Re*-face stereocenter and a *Si*-face stereocenter at C-25[30,107]. Considering that methyl transfer is a driving step in the cascade reactions and that methyl acceptors and donors must adopt a proper distance, the *Re*-face stereocenter was discerned as the dominant stereocenter. The proposed mechanism of action of TleD is that methyl transfer occurs first, and then, the carbocation is formed to initiate the subsequent cyclization (Scheme 5B). The hydrophobic pocket strictly ensures the occurrence of the correct methyl transformation and substrate orientation. Additionally, TleD shows very low or even no sequence identity with class I MTases but is closely homologous to SpnF, a SAM-MTase-like enzyme that catalyzes [4+2] cycloaddition that potentially proceeds through the Diels–Alder mechanism[31,108,109] (Scheme 5C). Structural comparison showed that the additional N-terminal α-helix is a common feature of MTase-like cyclases in TleD and SpnF, tightly anchoring the hydrophobic active site for catalysis (Fig. 5A and B).

Pericyclic reactions are the most powerful strategy for the formation of multiple regioselective and stereoselective carbon centers and are widely applied in the total synthesis of bioactive complexes[110]. Due to the lack of biosynthetic pericyclic reactions in natural product synthesis, the natural synthetic pathway of leporin has attracted much attention[111−113]. In 2017, the SAM-dependent dehydratase and multifunctional pericyclase LepI was identified[114]; this enzyme is responsible for the formation of the dihydropyran core of leporin *via* a bifurcated mechanism. LepI shares structural homology with several class I *O*-MTases, such as OxaC[115], mitomycin-7-*O*-methyltransferase[116], and PhzM[117]. LepI catalyzed pericyclization converges bifurcated reactions, including an E2-like anti-elimination dehydration, an intramolecular Diels–Alder (IMDA) reaction and hetero-Diels–Alder (HDA) reaction occurring *via* an ambimodal transition state, and a retro-Claisen rearrangement, to form one desired product (Scheme 5D). Neutrally charged SAH is found to inhibit the reaction, while positively charged SAM and sinefungin activate the enzyme[32,118]. 5′-Deoxy-5′-(methylthio) adenosine (MTA) also shows inhibitory effects and was confirmed as occupying the substrate-binding site by structural analysis[118]. To gain further insight into the structural mechanism and into the regulatory effects of SAH and sinefungin, the structures of LepI and its complexes were determined successively[32,118−120]. LepI forms a homodimer in an asymmetric form mediated by a domain-swapped N-terminal domain, and one of the helices is involved in hiding the surface of the active site in another subunit (Fig. 5C). Several bulky and hydrophobic residues have been observed to eliminate water and create a large hydrophobic cavity for substrate accommodation. Adjacent to SAM is a wide substrate entry tunnel, and many water-filled tunnels are observed on the backside of the cavity at the domain interface. LepI catalyzes dehydration through an anti-elimination mechanism, in which His133 acts as a general base to deprotonate 4-OH and Arg295 in the *trans* conformation to assist the release of the anti-periplanar OH group (Scheme 5D). Second, in the subsequent cycloaddition, a bond rotation of the diene occurs to improve shape complementarity in the active site. Endo TS-1 is subsequently generated with a low-energy conformation derived from the reactive geometry and by aligning hydrophilic residues, His133 and Arg295 in particular. This product then branches into two pathways, namely, direct HDA reaction and indirect IMDA reaction, to form the final product. Through the IMDA pathway, an endo adduct is generated, and the endo product is converted to the final product leporin C through a highly polarized TS-2 followed by retro-Claisen rearrangement, which is electrostatically established by the positively charged imidazolium of His133. LepI eliminates water molecules and stabilizes boat-like TS-2 by reducing the energy of rearrangement and changing the electronic properties of the substrate utilizing the cationic residues His133, Arg197 and Arg295 in the final step[118]. Notably, although the adjacent cofactor SAM does not directly interact with the substrate or contribute any allosteric effects, it defines the active site binding environment *via* the electrostatic effect of sulfonium or the ammonium analog and stabilizes the highly polarized TS-2[32]. This novel role of SAM is called "electric field catalysis"[121−125]. A parallel pattern is also observed in SlnM[29] and RdmB[21]. Another SAM-dependent pericyclase, SpnF, catalyzes the [4+2] cycloaddition[31], in which Tyr23 and Glu152 serve as a lid to anchor the active site. Despite several studies about SpnF[108,126,127], the role of SAM and further details are still unknown. Further understanding of the molecular mechanism of these enzymes might prompt the design of versatile and efficient pericyclases.

3.4. *Methylation, dehydrogenation and chelation*

CysG is a multifunctional enzyme from *S. enterica* that catalyzes three steps in the biosynthesis of siroheme and seems to be the prototypical siroheme synthase since it is the only enzyme involved in transforming uro'gen III to siroheme. CysG forms a homodimer, catalyzing three reactions: SAM-dependent tetrapyrrole C-2 and C-7 methylations from uroporphyrinogen III to precorrin-2, NAD^+-dependent tetrapyrrole dehydrogenation and metal chelation[128,129] (Scheme 6A). In *Bacillus megaterium*, CysG is separated into three enzymes: the SAM-dependent uro'gen III methyltransferase (SUMT) SirA, precorrin-2 dehydrogenase SirC and sirohydrochlorin ferrochelatase SirB[130]. In *Saccharomyces cerevisiae*, there are only two proteins, namely, Met1p (functioning as MTase) and Met8p (functioning as both dehydrogenase and ferro-chelatase)[131]. Additionally, as a member of the extended class III MTase family, $CysG^A$ showed 25% and 45% sequence identity with CbiF and CobA respectively and is homologous to CbiE[132] (Fig. 6A and B). CysG and its homologs control the branchpoint in the biosynthesis of siroheme or cobalamin (Fig. 6A). CysG forms a homodimer, and two functional domains are linked by a flexible loop[128] (Fig. 6C), named $CysG^A$ (residues 214−457, containing domains I^A and II^A and cofactor SAM; homologous to SirA and Metlp[33]) and $CysG^B$ (residues 1−213, containing domains I^B, II^B and III^B and cofactor NAD^+; homologous to Met8p and SirC[33]). SUMT shows similarity with the class III MTases-like $CysG^A$ domain, except in some extended loops in SUMT[133]. In the opposite position of the polypeptide chain of the CysG dimer, the cofactor NAD^+ is located at the edge of domain I^B, and its nicotinamide group inserts itself into the cleft formed by I^B and III^B. Another critical finding for the enzymes is the novel posttranslational modification of phosphor-Ser128 projecting into the active site of $CysG^B$, the S128D variant of which destroys the dehydrogenation or/and

ferrochelation function but without dysfunction of dimethylation activity. This enzyme is similar to isocitrate dehydrogenase, which is also regulated by phosphorylation at serine[134,135]. This might be interpreted as the addition of negatively charged phosphate conflicting with precorrin-2, which is full of negatively charged carboxyl groups, leading to low affinity of the substrate. This finding of selective elimination in the appointed function can further be used to engineer proteins for biocatalysis. The homolog of $CysG^B$ has also been studied[136–138]. Comparison of SirC, Met8p and CysG showed that the NAD-bound active site adopts various conformations. Arg159 is positioned in the active-site cleft in SirC, but the relevant arginine is located away from the active sites of CysG and Met8p[137]. It is also confusing that SirC, a dehydrogenase without chelatase activity, is found to bind Co(II) and Cu(II) in the same manner as Met8p, and this observation needs to be further explored to determine the requirements for chelatase activity[137].

3.5. *Methylation, epoxidation and isomerization*

Pseurotin A is a member of the pseurotin family, which exhibits a wide variety of bioactivities, such as inhibition of immunoglobulin E production[139] and induction of cell differentiation in PC12 cells[140]. The great significance of pseurotin A comes from the skeleton containing the spiro-ring core structure and the closely related compounds azaspirene and synerazol. In the main step of the pseurotin biosynthetic pathway, the conversion from the foremost precursor azaspirene to pseurotin A is realized by PsoF[34]. PsoF was initially found to be a bifunctional fusion protein that catalyzes C-methylation and epoxidation by the methyltransferase (MT) domain and FAD-containing monooxygenase (FMO) domain, respectively[34]. The enzyme CTB3 was also found in *Cercospora nicotianae*[141]. To study PsoF-MT, the analog *N*-acetylcysteamine (NAC) thioester was used to mimic the natural substrate. Methylated polyketide was observed in *trans-*

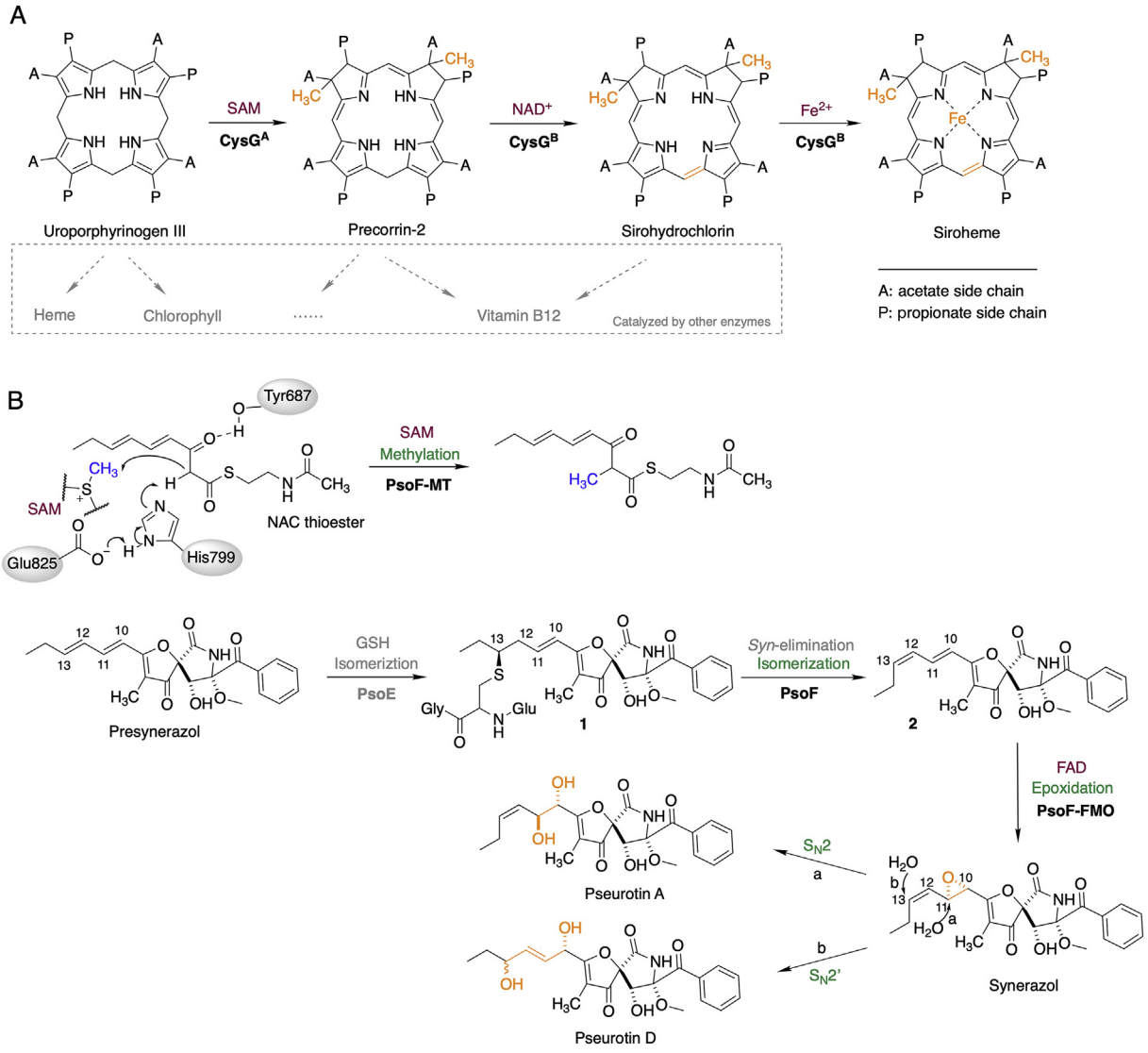

Scheme 6 Reactions catalyzed by CysG and PsoF. (A) Biosynthesis of siroheme catalyzed by CysG and branch pathways from the intermediates catalyzed by other enzymes. (B) Three reactions catalyzed by PsoF in the biosynthesis of pseurotin. Methylation is separated from isomerization and epoxidation in the biosynthesis cascade. Proposed electron transfers are indicated by curved arrows. PsoF-MT, methyltransferase domain of PsoF; PsoF-FMO, FAD-containing monooxygenase domain.

orientation[34]. The FMO domain is responsible for stereospecific epoxidation of C-10,11. Then, C-11 and C-13 are further non-enzymatically attacked by water molecules through the S_N2 or S_N2' mechanism to obtain the diol isomer (Scheme 6B). Another study also revealed that PsoF played a role in the *trans*-to-*cis* isomerization of C12−C13 in the PsoE-associated pathway intermediate presynerazol, making it a trifunctional enzyme[142]. As proposed, the PsoF-FMO domain oxidizes the sulfur atom of **1** followed by *syn*-elimination, which releases glutathione (GSH) to yield stereoisomer **2**. The *cis*-containing intermediate **2** remains in the active site and undergoes subsequent epoxidation. Unlike other multifunctional enzymes that catalyze consecutive reactions[143], it is unusual that PsoF does not adopt a consecutive mechanism of action and instead takes up two unrelated steps in the cascade[34]. This may be explained by the selectivity of the FMO domain, which favors an extensive polyketide chain with phenylalanine and possibly a spiro-ring, and such compounds are downstream of the pathway and fit in the substrate cavity of PsoF-FMO.

4. Conservation and diversity of SAM-dependent enzymes

Rossmann fold is the key feature of class I MTases, which occurs repeatedly in a large number of SAM-binding enzymes including the non-methyltransferases. Therefore, the structural conservation and catalytical diversity of class I-like non-methylating SAM-dependent enzymes are further explored in our review, while radical SAM enzymes have been comprehensively discussed[35–40] and are not included here.

The relevance of the class I-like non-methylating SAM-dependent enzymes has been analyzed from the sequences, structures and catalytic traits. The structure-based sequence alignment analysis[144] shows that the regions containing Rossmann fold are generally well aligned, and most of the critical residues interacting with SAM or stabilizing the Rossmann fold structure in characterized motifs[102] are identified (Fig. 7). Similar to the MTases[102], the acidic residues (Asp/Glu colored in green) and glycine-rich fragments (colored in blue) in motif I are highly conserved, which polarize water molecules and interact with carboxypropyl moieties of SAMs, respectively. The Asp/Glu acidic residues in motif IV, hydrophobic residues at the end of motif V and glycine in motif VI are partially conserved, with one or two exceptions. However, the acidic residues in motif II and motif III are absent in non-methyltransferases, while they are conserved in the typical Rossmann-fold MTases which interact with adenosyl base of SAM molecule. The absence of the acidic residues in motif II and III may represent the evolutionary diversity of the non-methyltransferases in the binding modes of SAM and ultimately end up with distinct catalytic reactions and functional promiscuities. Because the methylating and non-methylating reactions share distinct mechanisms to initialize the catalysis and the different chemical relativities of the substrates also require diverse circumstances of the binding pockets, it is difficult to draw any further marker in the sequence divergence to label the capability of catalysis and substrate specificity among the SAM-dependent enzymes.

The structural similarity of structurally-reported non-methyltransferases[21,25–27,30–32] has been analyzed using Dali server[145]. As expected, they share highly conserved Rossmann fold in C-terminus and a distinct N-terminus. The variable N-terminus plays diverse roles in dimerization, substrate specificity, or other functions, which results in the wide range of RMSD values ranging from 3.1 to 6.2 when taking RdmB as the reference structure.

Through the simple meta-analysis of the class I-like non-methylating SAM-dependent enzymes, some of them show

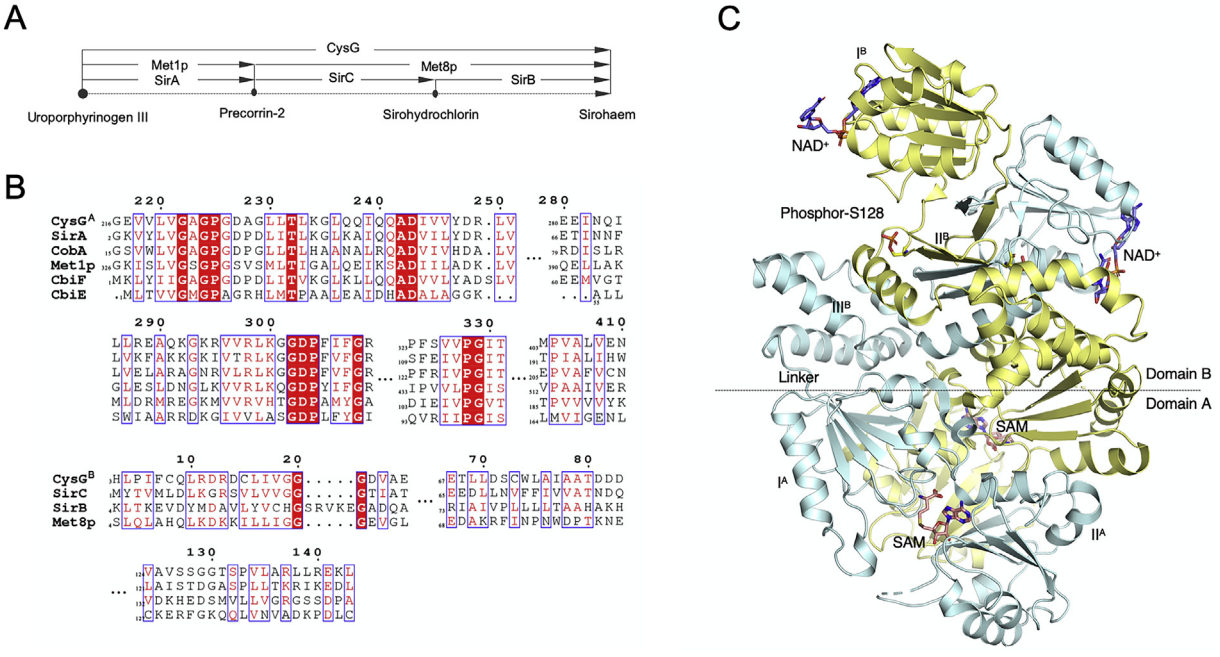

Figure 6 (A) Homology with CysG and reactions catalyzed by each enzyme. (B) Sequence alignment for $CysG^A$ and $CysG^B$ and their homologies. Some of the shared folds and SAM binding motifs are shown[128]. The alignment is performed by CLUSTALW and edited by ESPript[61]. (C) Overall structure of CysG (PDB: 1PJS). The two domains containing NAD^+ and SAM in each subunit are shown as domain A and domain B, roughly divided by the dashed line. The light-yellow subunit is labeled with domains I^B, II^B and III^B in domain B, and the light-cyan subunit is labeled with domains I^A and II^A. NAD^+ is colored purple; SAM is colored pink; phosphor-Ser128 is colored yellow and red.

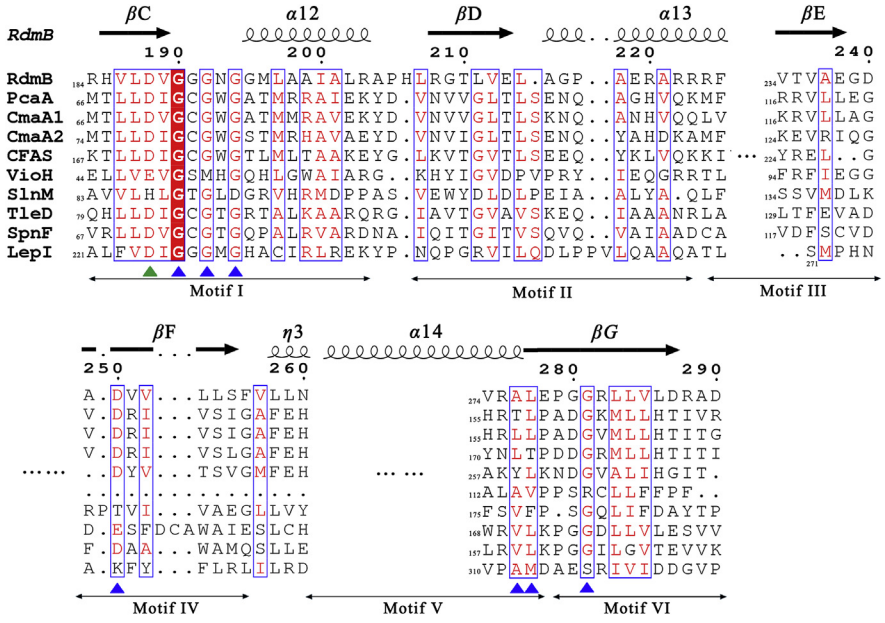

Figure 7 Structural-based sequence alignment of non-methylating SAM-dependent enzymes shows class I MTases core domains, which catalyzes non-methylations or multiple reactions without radical SAM. Triangles indicate the conserved/partial conserved residues in motifs for SAM binding[102]. The alignment is performed by T-Coffee[144] and edited by ESPript[61].

consistency in function and evolutionary relationship. Except for the acidic residues in motif II and III, most of them exhibit the invariant key residues in Rossmann fold for SAM binding. However, the role of other conserved or variant residues is still less understood. The SAM-dependent enzymes mentioned are "tailored to function". Galperin and Koonin[146] used the term "entatic state", that is "a catalytically poised state", to discuss the evolutionary relationship and the interplay of common and unique features among enzymes, which was originally proposed in 1968[147]. The class I MTases and class I-like non-methylating SAM-dependent enzymes in this review commonly share similar poised states preserved by the conservation of specific residues, while other variant residues are responsible for catalytic specificity of the enzymes, leading to distinct transition states for different reactions. That is to say, during evolution, the random mutations of amino acids in canonical Rossmann folds contribute to the diversity of enzymes, but not all the new entatic state of the protein is stable, and only the minority of neo-folded protein are viable which may reserve the main feature of Rossmann fold and mechanism[13]. Consequently, it is necessary to attach importance on the experimental characterization to correctly annotate the function of enzymes with the canonical domain.

5. Conclusions and outlook

The abundant evidence for SAM-dependent enzymes reviewed here apparently reveals the tailored functions and prolific substrate acceptance of these conserved class I MTase structures, which is referred to as catalytic promiscuity. Nonmethylation can be directly or indirectly dependent on SAM. In reactions that directly depend on SAM, such as cyclopropanation, SAM provides the methylene group through the S_N2-like or RS mechanism. On the other hand, in RdmB[21], SlnM[29] and LepI[32,118–120], SAM does not sacrifice itself but acts as an electron stabilizer through its positively charged sulfur center, which is reminiscent of "electric field catalysis"[121–125]. Some SAM-dependent enzymes catalyze methylation and other reactions by two discrete domains with different cofactors. For example, CysG catalyzes methylation, dehydrogenation and metal chelation though two domains in the opposite direction[128]; PsoF catalyzes methylation, isomerization and epoxidation through the MTase domain and FAD-containing monooxygenase (FMO) domain[34]. These enzymes may have a "switch" to lock or release functions. For example, epigenetic modification of serine in CysG can lock the activity of the FAD-containing domain.

These facts indicate the great potential of engineering SAM enzymes to generate new enzymes with pluripotency and conversion functions. The conversion of MTase to monooxygenase is a good example[66]. By comparing the key residues in DnrK and its homolog RdmB, a crucial phenylalanine in RdmB could serve as a gate to prevent water from entering the active site (Fig. 4). Thus, an amino acid was inserted into DnrK to reorient the phenylalanine in wild-type DnrK. The small alteration dramatically eliminated the MTase activity of DnrK and converted the enzyme to a monooxygenase (Scheme 2B).

Compared to chemical synthesis, enzymatic synthesis is a versatile method to obtain products with high chemo-, regio- and stereo-specificity. Enzymes accelerate reactions through stabilization of intermediates and products, resulting in preferred dynamics and thermodynamics. Due to the predominant roles of natural products in biomedical research, these groups of SAM-dependent enzymes might be good candidates for biocatalysis and cascade reactions in drug synthesis. Further investigation on the structure, molecular basis and biological functions of these enzymes is likely to spur significant advances in enzyme engineering and future application in a wide range of biosynthesis.

Acknowledgments

This work was supported by the National Natural Science Foundation of China (Grant No. 21702141).

Author contributions

Qiu Sun and Mengyuan Huang generated the manuscript draft. Yuquan Wei edited and revised the manuscript. All authors reviewed and approved the final version of the manuscript.

Conflicts of interest

The authors have no conflicts of interest to declare.

References

1. Cantoni GL. Biological methylation: selected aspects. *Annu Rev Biochem* 1975;**44**:435−51.
2. Chen H, Wang Z, Cai H, Zhou C. Progress in the microbial production of *S*-adenosyl-L-methionine. *World J Microbiol Biotechnol* 2016;**32**:153.
3. Greer EL, Shi Y. Histone methylation: a dynamic mark in health, disease and inheritance. *Nat Rev Genet* 2012;**13**:343−57.
4. He C. Grand challenge commentary: RNA epigenetics?. *Nat Chem Biol* 2010;**6**:863−5.
5. Goll MG, Bestor TH. Eukaryotic cytosine methyltransferases. *Annu Rev Biochem* 2005;**74**:481−514.
6. Arrowsmith CH, Bountra C, Fish PV, Lee K, Schapira M. Epigenetic protein families: a new frontier for drug discovery. *Nat Rev Drug Discov* 2012;**11**:384−400.
7. Qazi TJ, Quan Z, Mir A, Qing H. Epigenetics in Alzheimer's disease: perspective of DNA methylation. *Mol Microbiol* 2018;**55**:1026−44.
8. Newman DJ, Cragg GM. Natural products as sources of new drugs over the 30 years from 1981 to 2010. *J Nat Prod* 2012;**75**:311−35.
9. Talele TT. The "cyclopropyl fragment" is a versatile player that frequently appears in preclinical/clinical drug molecules. *J Med Chem* 2016;**59**:8712−56.
10. Garcia-Castro M, Zimmermann S, Sankar MG, Kumar K. Scaffold diversity synthesis and its application in probe and drug discovery. *Angew Chem Int Ed* 2016;**55**:7586−605.
11. Zheng Y, Tice CM, Singh SB. The use of spirocyclic scaffolds in drug discovery. *Bioorg Med Chem Lett* 2014;**24**:3673−82.
12. Shaaban MR, Mayhoub AS, Farag AM. Recent advances in the therapeutic applications of pyrazolines. *Expert Opin Ther Pat* 2012;**22**:253−91.
13. Liscombe DK, Louie GV, Noel JP. Architectures, mechanisms and molecular evolution of natural product methyltransferases. *Nat Prod Rep* 2012;**29**:1238−50.
14. Struck AW, Thompson ML, Wong LS, Micklefield J. *S*-adenosylmethionine-dependent methyltransferases: highly versatile enzymes in biocatalysis, biosynthesis and other biotechnological applications. *Chembiochem* 2012;**13**:2642−55.
15. Bennett MR, Shepherd SA, Cronin VA, Micklefield J. Recent advances in methyltransferase biocatalysis. *Curr Opin Chem Biol* 2017;**37**:97−106.
16. Luo H, Hansen ASL, Yang L, Schneider K, Kristensen M, Christensen U, et al. Coupling *S*-adenosylmethionine-dependent methylation to growth: design and uses. *PLoS Biol* 2019;**17**. e2007050.
17. Nelson JT, Lee J, Sims JW, Schmidt EW. Characterization of SafC, a catechol 4-*O*-methyltransferase involved in saframycin biosynthesis. *Appl Environ Microbiol* 2007;**73**:3575−80.
18. Malla S, Koffas MAG, Kazlauskas RJ, Kim BG. Production of 7-*O*-methyl aromadendrin, a medicinally valuable flavonoid, in *Escherichia coli*. *Appl Environ Microbiol* 2012;**78**:684−94.
19. Grobe N, Ren X, Kutchan TM, Zenk MH. An (*R*)-specific *N*-methyltransferase involved in human morphine biosynthesis. *Arch Biochem Biophys* 2011;**506**:42−7.
20. Layer G, Moser J, Heinz DW, Jahn D, Schubert WD. Crystal structure of coproporphyrinogen III oxidase reveals cofactor geometry of Radical SAM enzymes. *EMBO J* 2003;**22**:6214−24.
21. Jansson A, Niemi J, Lindqvist Y, Mäntsälä P, Schneider G. Crystal structure of aclacinomycin-10-hydroxylase, a *S*-adenosyl-L-methionine-dependent methyltransferase homolog involved in anthracycline biosynthesis in *Streptomyces purpurascens*. *J Mol Biol* 2003;**334**:269−80.
22. LaMattina JW, Nix DB, Lanzilotta WN. Radical new paradigm for heme degradation in *Escherichia coli* O157:H7. *Proc Natl Acad Sci U S A* 2016;**113**:12138−43.
23. Layer G, Verfürth K, Mahlitz E, Jahn D. Oxygen-independent coproporphyrinogen-III oxidase HemN from *Escherichia coli*. *J Biol Chem* 2002;**277**:34136−42.
24. Wu S, Jian XH, Yuan H, Jin WB, Yin Y, Wang LY, et al. Unified biosynthetic origin of the benzodipyrrole subunits in CC-1065. *ACS Chem Biol* 2017;**12**:1603−10.
25. Huang CC, Smith CV, Glickman MS, Jacobs WR, Sacchettini JC. Crystal structures of mycolic acid cyclopropane synthases from *Mycobacterium tuberculosis*. *J Biol Chem* 2002;**277**:11559−69.
26. Ma Y, Pan C, Wang Q. Crystal structure of bacterial cyclopropane-fatty-acyl-phospholipid synthase with phospholipid. *J Biochem* 2019;**166**:139−47.
27. Hari SB, Grant RA, Sauer RT. Structural and functional analysis of *E. coli* cyclopropane fatty acid synthase. *Structure* 2018;**26**:1251−1258.e3.
28. Yan F, Muller R. Class I methyltransferase VioH catalyzes unusual *S*-adenosyl-L-methionine cyclization leading to 4-methylazetidinecarboxylic acid formation during vioprolide biosynthesis. *ACS Chem Biol* 2019;**14**:99−105.
29. Jiang C, Qi Z, Kang Q, Liu J, Jiang M, Bai L. Formation of the $\Delta^{18,19}$ double bond and bis(spiroacetal) in salinomycin is atypically catalyzed by SlnM, a methyltransferase-like enzyme. *Angew Chem Int Ed* 2015;**54**:9097−100.
30. Yu F, Li M, Xu C, Sun B, Zhou H, Wang Z, et al. Crystal structure and enantioselectivity of terpene cyclization in SAM-dependent methyltransferase TleD. *Biochem J* 2016;**473**:4385−97.
31. Fage CD, Isiorho EA, Liu Y, Wagner DT, Liu HW, Keatinge-Clay AT. The structure of SpnF, a standalone enzyme that catalyzes [4+2] cycloaddition. *Nat Chem Biol* 2015;**11**:256−8.
32. Cai Y, Hai Y, Ohashi M, Jamieson CS, Garcia-Borras M, Houk KN, et al. Structural basis for stereoselective dehydration and hydrogen-bonding catalysis by the SAM-dependent pericyclase LepI. *Nat Chem* 2019;**11**:812−20.
33. Warren MJ, Bolt EL, Roessner CA, Scott AI, Spencer JB, Woodcock SC. Gene dissection demonstrates that the *Escherichia coli* cysG gene encodes a multifunctional protein. *Biochem J* 1994;**302**:837−44.
34. Tsunematsu Y, Fukutomi M, Saruwatari T, Noguchi H, Hotta K, Tang Y, et al. Elucidation of pseurotin biosynthetic pathway points to *trans*-acting *C*-methyltransferase: generation of chemical diversity. *Angew Chem Int Ed* 2014;**53**:8475−9.
35. Broderick WE, Broderick JB. Radical SAM enzymes: surprises along the path to understanding mechanism. *J Biol Inorg Chem* 2019;**24**:769−76.
36. Broderick WE, Hoffman BM, Broderick JB. Mechanism of radical initiation in the radical *S*-adenosyl-L-methionine superfamily. *Acc Chem Res* 2018;**51**:2611−9.
37. Frey PA, Hegeman AD, Ruzicka FJ. The radical SAM superfamily. *Crit Rev Biochem Mol Biol* 2008;**43**:63−88.
38. Nicolet Y. Structure−function relationships of radical SAM enzymes. *Nat Catal* 2020;**3**:337−50.
39. Zhou S, Alkhalaf LM, de los Santos ELC, Challis GL. Mechanistic insights into class B radical-*S*-adenosylmethionine methylases: ubiquitous tailoring enzymes in natural product biosynthesis. *Curr Opin Chem Biol* 2016;**35**:73−9.
40. Ding W, Ji X, Zhong Y, Xu K, Zhang Q. Adenosylation reactions catalyzed by the radical *S*-adenosylmethionine superfamily enzymes. *Curr Opin Chem Biol* 2020;**55**:86−95.
41. Cheng X, Kumar S, Posfai J, Pflugrath JW, Roberts RJ. Crystal structure of the Hhal DNA methyltransferase complexed with *S*-adenosyl-L-methionine. *Cell* 1993;**74**:299−307.

42. Schubert HL, Blumenthal RM, Cheng X. Many paths to methyltransfer: a chronicle of convergence. *Trends Biochem Sci* 2003;**28**:329−35.
43. Vey JL, Drennan CL. Structural insights into radical generation by the radical SAM superfamily. *Chem Rev* 2011;**111**:2487−506.
44. Zubieta C, Ross JR, Koscheski P, Yang Y, Pichersky E, Noel JP. Structural basis for substrate recognition in the salicylic acid carboxyl methyltransferase family. *Plant Cell* 2003;**15**:1704−16.
45. Jansson A, Koskiniemi H, Mantsala P, Niemi J, Schneider G. Crystal structure of a ternary complex of DnrK, a methyltransferase in daunorubicin biosynthesis, with bound products. *J Biol Chem* 2004;**279**:41149−56.
46. Dai YN, Zhou K, Cao DD, Jiang YL, Meng F, Chi CB, et al. Crystal structures and catalytic mechanism of the *C*-methyltransferase Coq5 provide insights into a key step of the yeast coenzyme Q synthesis pathway. *Acta Crystallogr D Biol Crystallogr* 2014;**70**:2085−92.
47. Pavkov-Keller T, Steiner K, Faber M, Tengg M, Schwab H, Gruber-Khadjawi M, et al. Crystal structure and catalytic mechanism of CouO, a versatile C-methyltransferase from *Streptomyces rishiriensis*. *PLoS One* 2017;**12**. E0171056.
48. Frank S, Deery E, Brindley AA, Leech HK, Lawrence A, Heathcote P, et al. Elucidation of substrate specificity in the cobalamin (vitamin B12) biosynthetic methyltransferases. Structure and function of the C20 methyltransferase (CbiL) from *Methanothermobacter thermautotrophicus*. *J Biol Chem* 2007;**282**:23957−69.
49. Storbeck S, Saha S, Krausze J, Klink BU, Heinz DW, Layer G. Crystal structure of the heme d1 biosynthesis enzyme NirE in complex with its substrate reveals new insights into the catalytic mechanism of *S*-adenosyl-L-methionine-dependent uroporphyrinogen III methyltransferases. *J Biol Chem* 2011;**286**:26754−67.
50. Ferrer JL, Zubieta C, Dixon RA, Noel JP. Crystal structures of alfalfa caffeoyl coenzyme A 3-*O*-methyltransferase. *Plant Physiol* 2005;**137**:1009−17.
51. Zhang Q, van der Donk WA, Liu W. Radical-mediated enzymatic methylation: a tale of two SAMS. *Acc Chem Res* 2012;**45**:555−64.
52. Layer G, Grage K, Teschner T, Schunemann V, Breckau D, Masoumi A, et al. Radical *S*-adenosylmethionine enzyme coproporphyrinogen III oxidase HemN: functional features of the [4Fe-4S] cluster and the two bound *S*-adenosyl-L-methionines. *J Biol Chem* 2005;**280**:29038−46.
53. Layer G, Pierik AJ, Trost M, Rigby SE, Leech HK, Grage K, et al. The substrate radical of *Escherichia coli* oxygen-independent coproporphyrinogen III oxidase HemN. *J Biol Chem* 2006;**281**:15727−34.
54. Ji X, Mo T, Liu WQ, Ding W, Deng Z, Zhang Q. Revisiting the mechanism of the anaerobic coproporphyrinogen III oxidase HemN. *Angew Chem Int Ed* 2019;**58**:6235−8.
55. Goto T, Aoki R, Minamizaki K, Fujita Y. Functional differentiation of two analogous coproporphyrinogen III oxidases for heme and chlorophyll biosynthesis pathways in the cyanobacterium *Synechocystis sp.* PCC 6803. *Plant Cell Physiol* 2010;**51**:650−63.
56. Duwat P, Sourice S, Cesselin B, Lamberet G, Vido K, Gaudu P, et al. Respiration capacity of the fermenting bacterium *Lactococcus lactis* and its positive effects on growth and survival. *J Bacteriol* 2001;**183**:4509−16.
57. Haskamp V, Karrie S, Mingers T, Barthels S, Alberge F, Magalon A, et al. The radical SAM protein HemW is a heme chaperone. *J Biol Chem* 2018;**293**:2558−72.
58. Abicht HK, Martinez J, Layer G, Jahn D, Solioz M. *Lactococcus lactis* HemW (HemN) is a haem-binding protein with a putative role in haem trafficking. *Biochem J* 2012;**442**:335−43.
59. Bali S, Lawrence AD, Lobo SA, Saraiva LM, Golding BT, Palmer DJ, et al. Molecular hijacking of siroheme for the synthesis of heme and d1 heme. *Proc Natl Acad Sci U S A* 2011;**108**:18260−5.
60. Layer G, Reichelt J, Jahn D, Heinz DW. Structure and function of enzymes in heme biosynthesis. *Protein Sci* 2010;**19**:1137−61.
61. Robert X, Gouet P. Deciphering key features in protein structures with the new ENDscript server. *Nucleic Acids Res* 2014;**42**:W320−4.
62. Metsä-Ketelä M, Niemi J, Mäntsälä P, Schneider G. Anthracycline biosynthesis: genes, enzymes and mechanisms. In: Krohn K, editor. *Anthracycline chemistry and biology I. Topics in current chemistry*. Berlin, Heidelberg: Springer Berlin Heidelberg; 2008. p. 101−40.
63. Hutchinson CR. Biosynthetic studies of daunorubicin and tetracenomycin C. *Chem Rev* 1997;**97**:2525−36.
64. Pang B, Qiao X, Janssen L, Velds A, Groothuis T, Kerkhoven R, et al. Drug-induced histone eviction from open chromatin contributes to the chemotherapeutic effects of doxorubicin. *Nat Commun* 2013;**4**:1908.
65. Jansson A, Koskiniemi H, Erola A, Wang J, Mantsala P, Schneider G, et al. Aclacinomycin 10-hydroxylase is a novel substrate-assisted hydroxylase requiring *S*-adenosyl-L-methionine as cofactor. *J Biol Chem* 2005;**280**:3636−44.
66. Grocholski T, Dinis P, Niiranen L, Niemi J, Metsä-Ketelä M. Divergent evolution of an atypical *S*-adenosyl-L-methionine−dependent monooxygenase involved in anthracycline biosynthesis. *Proc Natl Acad Sci U S A* 2015;**112**:9866−71.
67. Grocholski T, Koskiniemi H, Lindqvist Y, Mäntsälä P, Niemi J, Schneider G. Crystal structure of the cofactor-independent monooxygenase SnoaB from *Streptomyces nogalater*: implications for the reaction mechanism. *Biochemistry* 2010;**49**:934−44.
68. Siitonen V, Blauenburg B, Kallio P, Mäntsälä P, Metsä-Ketelä M. Discovery of a two-component monooxygenase SnoaW/SnoaL2 involved in nogalamycin biosynthesis. *Chem Biol* 2012;**19**:638−46.
69. Thierbach S, Bui N, Zapp J, Chhabra Siri R, Kappl R, Fetzner S. Substrate-assisted O_2 activation in a cofactor-independent dioxygenase. *Chem Biol* 2014;**21**:217−25.
70. Fetzner S, Steiner RA. Cofactor-independent oxidases and oxygenases. *Appl Microbiol Biotechnol* 2010;**86**:791−804.
71. Hooda J, Shah A, Zhang L. Heme, an essential nutrient from dietary proteins, critically impacts diverse physiological and pathological processes. *Nutrients* 2014;**6**:1080−102.
72. Wilks A, Burkhard KA. Heme and virulence: how bacterial pathogens regulate, transport and utilize heme. *Nat Prod Rep* 2007;**24**:511−22.
73. Torres AG, Payne SM. Haem iron-transport system in enterohaemorrhagic *Escherichia coli* O157:H7. *Mol Microbiol* 1997;**23**:825−33.
74. Wyckoff EE, Schmitt M, Wilks A, Payne SM. HutZ is required for efficient heme utilization in *Vibrio cholerae*. *J Bacteriol* 2004;**186**:4142−51.
75. Dailey HA, Gerdes S, Dailey TA, Burch JS, Phillips JD. Noncanonical coproporphyrin-dependent bacterial heme biosynthesis pathway that does not use protoporphyrin. *Proc Natl Acad Sci U S A* 2015;**112**:2210−5.
76. Igarashi Y, Futamata K, Fujita T, Sekine A, Senda H, Naoki H, et al. Yatakemycin, a novel antifungal antibiotic produced by *Streptomyces* sp. TP-A0356. *J Antibiot* 2003;**56**:107−13 (Tokyo).
77. Tokoro Y, Isoe T, Shindo K. Gilvusmycin, a new antitumor antibiotic related to CC-1065. *J Antibiot* 1999;**52**:263−8.
78. Ichimura M, Ogawa T, Takahashi K, Kobayashi E, Kawamoto I, Yasuzawa T, et al. Duocarmycin SA, a new antitumor antibiotic from *Streptomyces* sp. *J Antibiot* 1990;**43**:1037−8.
79. Takahashi I, Takahashi K, Ichimura M, Morimoto M, Asano K, Kawamoto I, et al. Duocarmycin A, a new antitumor antibiotic from *Streptomyces*. *J Antibiot* 1988;**41**:1915−7.
80. Hanka LJ, Dietz A, Gerpheide SA, Kuentzel SL, Martin DG. CC-1065 (NSC-298223), a new antitumor antibiotic. Production, *in vitro* biological activity, microbiological assays and taxonomy of the producing microorganism. *J Antibiot* 1978;**31**:1211−7.
81. Tichenor MS, Boger DL. Yatakemycin: total synthesis, DNA alkylation, and biological properties. *Nat Prod Rep* 2008;**25**:220−6.

82. Boger DL, Garbaccio RM. Shape-dependent catalysis: insights into the source of catalysis for the CC-1065 and duocarmycin DNA alkylation reaction. *Acc Chem Res* 1999;**32**:1043−52.
83. Menderes G, Bonazzoli E, Bellone S, Black J, Predolini F, Pettinella F, et al. SYD985, a novel duocarmycin-based HER2-targeting antibody−drug conjugate, shows antitumor activity in uterine and ovarian carcinosarcoma with HER2/Neu expression. *Clin Canc Res* 2017;**38**:5836−45.
84. Thomas A, Teicher BA, Hassan R. Antibody-drug conjugates for cancer therapy. *Lancet Oncol* 2016;**17**:E254−62.
85. Tietze LF, Krewer B. Novel analogues of CC-1065 and the duocarmycins for the use in targeted tumour therapies. *Anti Canc Agents Med Chem* 2009;**9**:304−25.
86. Chen DYK, Pouwer RH, Richard JA. Recent advances in the total synthesis of cyclopropane-containing natural products. *Chem Soc Rev* 2012;**41**:4631−42.
87. Huang W, Xu H, Li Y, Zhang F, Chen XY, He QL, et al. Characterization of yatakemycin gene cluster revealing a radical *S*-adenosylmethionine dependent methyltransferase and highlighting spirocyclopropane biosynthesis. *J Am Chem Soc* 2012;**134**:8831−40.
88. Jin WB, Wu S, Jian XH, Yuan H, Tang GL. A radical *S*-adenosyl-L-methionine enzyme and a methyltransferase catalyze cyclopropane formation in natural product biosynthesis. *Nat Commun* 2018;**9**:2771.
89. Hiratsuka T, Suzuki H, Kariya R, Seo T, Minami A, Oikawa H. Biosynthesis of the structurally unique polycyclopropanated polyketide-nucleoside hybrid jawsamycin (FR-900848). *Angew Chem Int Ed* 2014;**53**:5423−6.
90. Tokiwano T, Watanabe H, Seo T, Oikawa H. Unprecedented biological cyclopropanation in the biosynthesis of FR-900848. *Chem Commun* 2008:6016−8.
91. Defelipe LA, Osman F, Marti MA, Turjanski AG. Structural and mechanistic comparison of the cyclopropane mycolic acid synthases (CMAS) protein family of *Mycobacterium tuberculosis*. *Biochem Biophys Res Commun* 2018;**498**:288−95.
92. Liao RZ, Georgieva P, Yu JG, Himo F. Mechanism of mycolic acid cyclopropane synthase: a theoretical study. *Biochemistry* 2011;**50**:1505−13.
93. Iwig DF, Uchida A, Stromberg JA, Booker SJ. The activity of *Escherichia coli* cyclopropane fatty acid synthase depends on the presence of bicarbonate. *J Am Chem Soc* 2005;**127**:11612−3.
94. Iwig DF, Grippe AT, McIntyre TA, Booker SJ. Isotope and elemental effects indicate a rate-limiting methyl transfer as the initial step in the reaction catalyzed by *Escherichia coli* cyclopropane fatty acid synthase. *Biochemistry* 2004;**43**:13510−24.
95. Schummer D, Höfle G, Forche E, Reichenbach H, Wray V, Domke T. Antibiotics from gliding bacteria, LXXVI. Vioprolides: new antifungal and cytotoxic peptolides from *Cystobacter violaceus*. *Liebigs Ann* 1996;**1996**:971−8.
96. Wu G, Nielson JR, Peterson RT, Winter JM. Bonnevillamides, linear heptapeptides isolated from a great salt lake-derived *Streptomyces sp*. *Mar Drugs* 2017;**15**.
97. Yan F, Auerbach D, Chai Y, Keller L, Tu Q, Huttel S, et al. Biosynthesis and heterologous production of vioprolides: rational biosynthetic engineering and unprecedented 4-methylazetidinecarboxylic acid formation. *Angew Chem Int Ed* 2018;**57**:8754−9.
98. Gupta PB, Onder TT, Jiang G, Tao K, Kuperwasser C, Weinberg RA, et al. Identification of selective inhibitors of cancer stem cells by high-throughput screening. *Cell* 2009;**138**:645−59.
99. Gallimore AR. The biosynthesis of polyketide-derived polycyclic ethers. *Nat Prod Rep* 2009;**26**:266−80.
100. Riddell FG. Structure, conformation, and mechanism in the membrane transport of alkali metal ions by ionophoric antibiotics. *Chirality* 2002;**14**:121−5.
101. Decker H, Motamedi H, Hutchinson CR. Nucleotide sequences and heterologous expression of tcmG and tcmP, biosynthetic genes for tetracenomycin C in *Streptomyces glaucescens*. *J Bacteriol* 1993;**175**:3876−86.
102. Kozbial PZ, Mushegian AR. Natural history of *S*-adenosylmethionine-binding proteins. *BMC Struct Biol* 2005;**5**:19.
103. Martin JL, McMillan FM. SAM (dependent) I AM: the *S*-adenosylmethionine-dependent methyltransferase fold. *Curr Opin Chem Biol* 2002;**12**:783−93.
104. Fujiki H, Mori M, Nakayasu M, Terada M, Sugimura T, Moore RE. Indole alkaloids: dihydroteleocidin B, teleocidin, and lyngbyatoxin A as members of a new class of tumor promoters. *Proc Natl Acad Sci U S A* 1981;**78**:3872−6.
105. Thoma R, Schulz-Gasch T, D'Arcy B, Benz J, Aebi J, Dehmlow H, et al. Insight into steroid scaffold formation from the structure of human oxidosqualene cyclase. *Nature* 2004;**432**:118−22.
106. Wendt KU, Poralla K, Schulz GE. Structure and function of a squalene cyclase. *Science* 1997;**277**:1811−5.
107. Awakawa T, Zhang L, Wakimoto T, Hoshino S, Mori T, Ito T, et al. A methyltransferase initiates terpene cyclization in teleocidin B biosynthesis. *J Am Chem Soc* 2014;**136**:9910−3.
108. Jeon BS, Ruszczycky MW, Russell WK, Lin GM, Kim N, Choi Sh, et al. Investigation of the mechanism of the SpnF-catalyzed [4+2]-cycloaddition reaction in the biosynthesis of spinosyn A. *Proc Natl Acad Sci U S A* 2017;**114**:10408−13.
109. Yang Z, Yang S, Yu P, Li Y, Doubleday C, Park J, et al. Influence of water and enzyme SpnF on the dynamics and energetics of the ambimodal [6+4]/[4+2] cycloaddition. *Proc Natl Acad Sci U S A* 2018;**115**:E848−55.
110. Hoffmann R, Woodward RB. Conservation of orbital symmetry. *Acc Chem Res* 1968;**1**:17−22.
111. Tang MC, Zou Y, Watanabe K, Walsh CT, Tang Y. Oxidative cyclization in natural product biosynthesis. *Chem Rev* 2017;**117**:5226−333.
112. Lin CI, McCarty RM, Liu HW. The enzymology of organic transformations: a survey of name reactions in biological systems. *Angew Chem Int Ed* 2017;**56**:3446−89.
113. Minami A, Oikawa H. Recent advances of Diels–Alderases involved in natural product biosynthesis. *J Antibiot* 2016;**69**:500−6.
114. Ohashi M, Liu F, Hai Y, Chen M, Tang MC, Yang Z, et al. SAM-dependent enzyme-catalysed pericyclic reactions in natural product biosynthesis. *Nature* 2017;**549**:502−6.
115. Newmister SA, Romminger S, Schmidt JJ, Williams RM, Smith JL, Berlinck RGS, et al. Unveiling sequential late-stage methyltransferase reactions in the meleagrin/oxaline biosynthetic pathway. *Org Biomol Chem* 2018;**16**:6450−9.
116. Singh S, Chang A, Goff RD, Bingman CA, Grüschow S, Sherman DH, et al. Structural characterization of the mitomycin 7-*O*-methyltransferase. *Proteins* 2011;**79**:2181−8.
117. Jiang J, Guiza Beltran D, Schacht A, Wright S, Zhang L, Du L. Functional and structural analysis of phenazine *O*-methyltransferase LaPhzM from *Lysobacter antibioticus* OH13 and one-pot enzymatic synthesis of the antibiotic myxin. *ACS Chem Biol* 2018;**13**:1003−12.
118. Sun Q, Hu Y, Gu Y, Huang J, He J, Luo L, et al. Deciphering the regulatory and catalytic mechanisms of an unusual SAM-dependent enzyme. *Signal Transduct Target Ther* 2019;**4**:17.
119. Chang Z, Ansbacher T, Zhang L, Yang Y, Ko TP, Zhang G, et al. Crystal structure of LepI, a multifunctional SAM-dependent enzyme which catalyzes pericyclic reactions in leporin biosynthesis. *Org Biomol Chem* 2019;**17**:2070−6.
120. Chang M, Zhou Y, Wang H, Liu Z, Zhang Y, Feng Y. Crystal structure of the multifunctional SAM-dependent enzyme LepI provides insights into its catalytic mechanism. *Biochem Biophys Res Commun* 2019;**515**:255−60.
121. Warshel A, Sharma PK, Kato M, Xiang Y, Liu H, Olsson MH. Electrostatic basis for enzyme catalysis. *Chem Rev* 2006;**106**:3210−35.
122. Welborn VV, Ruiz Pestana L, Head-Gordon T. Computational optimization of electric fields for better catalysis design. *Nat Catal* 2018;**1**:649−55.
123. Fried SD, Boxer SG. Electric fields and enzyme catalysis. *Annu Rev Biochem* 2017;**86**:387−415.

124. Shaik S, Mandal D, Ramanan R. Oriented electric fields as future smart reagents in chemistry. *Nat Chem* 2016;**8**:1091−8.
125. Aragonès AC, Haworth NL, Darwish N, Ciampi S, Bloomfield NJ, Wallace GG, et al. Electrostatic catalysis of a Diels–Alder reaction. *Nature* 2016;**531**:88−91.
126. Medvedev MG, Zeifman AA, Novikov FN, Bushmarinov IS, Stroganov OV, Titov IY, et al. Quantifying possible routes for SpnF-catalyzed formal Diels–Alder cycloaddition. *J Am Chem Soc* 2017;**139**:3942−5.
127. Patel A, Chen Z, Yang Z, Gutiérrez O, Liu HW, Houk KN, et al. Dynamically complex [6+4] and [4+2] cycloadditions in the biosynthesis of spinosyn A. *J Am Chem Soc* 2016;**138**:3631−4.
128. Stroupe ME, Leech HK, Daniels DS, Warren MJ, Getzoff ED. CysG structure reveals tetrapyrrole-binding features and novel regulation of siroheme biosynthesis. *Nat Struct Biol* 2003;**10**:1064−73.
129. Pennington JM, Kemp M, McGarry L, Chen Y, Stroupe ME. Siroheme synthase orients substrates for dehydrogenase and chelatase activities in a common active site. *Nat Commun* 2020;**11**:864.
130. Raux E, Leech HK, Beck R, Schubert HL, Santander PJ, Roessner CA, et al. Identification and functional analysis of enzymes required for precorrin-2 dehydrogenation and metal ion insertion in the biosynthesis of sirohaem and cobalamin in *Bacillus megaterium*. *Biochem J* 2003;**370**:505−16.
131. Raux E, McVeigh T, Peters SE, Leustek T, Warren MJ. The role of *Saccharomyces cerevisiae* Met1p and Met8p in sirohaem and cobalamin biosynthesis. *Biochem J* 1999;**338**:701−8.
132. Crouzet J, Cameron B, Cauchois L, Rigault S, Rouyez MC, Blanche F, et al. Genetic and sequence analysis of an 8.7-kilobase *Pseudomonas* denitrificans fragment carrying eight genes involved in transformation of precorrin-2 to cobyrinic acid. *J Bacteriol* 1990;**172**:5980−90.
133. Vevodova J, Graham RM, Raux E, Schubert HL, Roper DI, Brindley AA, et al. Structure/function studies on a *S*-adenosyl-L-methionine-dependent uroporphyrinogen III C methyltransferase (SUMT), a key regulatory enzyme of tetrapyrrole biosynthesis. *J Mol Biol* 2004;**344**:419−33.
134. Hurley JH, Dean AM, Sohl JL, Koshland Jr DE, Stroud RM. Regulation of an enzyme by phosphorylation at the active site. *Science* 1990;**249**:1012−6.
135. Dean AM, Koshland Jr DE. Electrostatic and steric contributions to regulation at the active site of isocitrate dehydrogenase. *Science* 1990;**249**:1044−6.
136. Schubert HL, Raux E, Brindley AA, Leech HK, Wilson KS, Hill CP, et al. The structure of *Saccharomyces cerevisiae* Met8p, a bifunctional dehydrogenase and ferrochelatase. *EMBO J* 2002;**21**:2068−75.
137. Schubert Heidi L, Rose Ruth S, Leech Helen K, Brindley Amanda A, Hill Christopher P, Rigby Stephen EJ, et al. Structure and function of SirC from *Bacillus megaterium*: a metal-binding precorrin-2 dehydrogenase. *Biochem J* 2008;**415**:257−63.
138. Fujishiro T, Shimada Y, Nakamura R, Ooi M. Structure of sirohydrochlorin ferrochelatase SirB: the last of the structures of the class II chelatase family. *Dalton Trans* 2019;**48**:6083−90.
139. Ishikawa M, Ninomiya T, Akabane H, Kushida N, Tsujiuchi G, Ohyama M, et al. Pseurotin A and its analogues as inhibitors of immunoglobuline E production. *Bioorg Med Chem Lett* 2009;**19**:1457−60.
140. Komagata D, Fujita S, Yamashita N, Saito S, Morino T. Novel neuritogenic activities of pseurotin A and penicillic acid. *J Antibiot (Tokyo)* 1996;**49**:958−9.
141. Dekkers KL, You BJ, Gowda VS, Liao HL, Lee MH, Bau HJ, et al. The *Cercospora nicotianae* gene encoding dual *O*-methyltransferase and FAD-dependent monooxygenase domains mediates cercosporin toxin biosynthesis. *Fungal Genet Biol* 2007;**44**:444−54.
142. Yamamoto T, Tsunematsu Y, Hara K, Suzuki T, Kishimoto S, Kawagishi H, et al. Oxidative *trans* to *cis* isomerization of olefins in polyketide biosynthesis. *Angew Chem Int Ed* 2016;**55**:6207−10.
143. Kim J, Almo SC. Structural basis for hypermodification of the wobble uridine in tRNA by bifunctional enzyme MnmC. *BMC Struct Biol* 2013;**13**:5.
144. Notredame C, Higgins DG, Heringa J. T-Coffee: a novel method for fast and accurate multiple sequence alignment. *J Mol Biol* 2000;**302**:205−17.
145. Holm L, Laakso LM. Dali server update. *Nucleic Acids Res* 2016;**44**:W351−5.
146. Galperin MY, Koonin EV. Divergence and convergence in enzyme evolution. *J Biol Chem* 2012;**287**:21−8.
147. Vallee BL, Williams RJ. Metalloenzymes: the entatic nature of their active sites. *Proc Natl Acad Sci U S A* 1968;**59**:498−505.